AFRL-AFOSR-VA-TR-2016-0046

CHARACTERIZATION AND BIOMIMCRY OF AVIAN NANOSTRUCTURED TISSUES

Matthew Shawkey
THE UNIVERSITY OF AKRON

01/19/2016
Final Report

Air Force Research Laboratory
AF Office Of Scientific Research (AFOSR)/ RTB2
Arlington, Virginia 22203
Air Force Materiel Command

REPORT DOCUMENTATION PAGE

Form Approved
OMB No. 0704-0188

PLEASE DO NOT RETURN YOUR FORM TO THE ABOVE ORGANIZATION.

1. REPORT DATE *(DD-MM-YYYY)*	2. REPORT TYPE	3. DATES COVERED *(From - To)*
05-01-2016	Final Report	September 2013-December 2015

4. TITLE AND SUBTITLE

CHARACTERIZATION AND BIOMIMCRY OF AVIAN NANOSTRUCTURED TISSUES

5a. CONTRACT NUMBER

5b. GRANT NUMBER

FA-9550-13-1-0222

5c. PROGRAM ELEMENT NUMBER

6. AUTHOR(S)

Matthew D. Shawkey

5d. PROJECT NUMBER

5e. TASK NUMBER

5f. WORK UNIT NUMBER

7. PERFORMING ORGANIZATION NAME(S) AND ADDRESS(ES)

University of Akron
Deaprtment of Biology
175 E. Mill St.
Akron, OH 44325-3908

8. PERFORMING ORGANIZATION REPORT NUMBER

9. SPONSORING/MONITORING AGENCY NAME(S) AND ADDRESS(ES)

AFOSR
875 N Randolph St Ste 3112
Arlington VA 22203

10. SPONSOR/MONITOR'S ACRONYM(S)

11. SPONSOR/MONITOR'S REPORT NUMBER(S)

12. DISTRIBUTION/AVAILABILITY STATEMENT

Publicly available

13. SUPPLEMENTARY NOTES

14. ABSTRACT

Understanding the properties and development of complex morphological traits may spark advances in the biomimetic design of new self-assembling multifunctional materials. Thus, we are using cutting-edge techniques to (I) identify previously unexplored chemical and physical properties of, and (II) synthetically mimic, color-producing nanostructures built from keratin and melanin in bird feathers.
For (I) we are testing four properties of optical nanostructures: (1) Refractive index and chemistry. (2) Tensile strength. (3) Thermoregulation. (4) Hydrophobicity. For part (II) we use biomimetic approaches to elucidate the mechanisms by which these nanostructures self assemble. We have succeeded in organizing melanin particles into simple nanostructures that are responsive to environmentalchanges, and are proceeding with experiments using blends and modified particle types. The results of this research will enhance our understanding of the multifunctionality of nanostructured traits and identify new means and natural materials for their production.

15. SUBJECT TERMS

Optics, photonics, nanostructure, self-assembly, colloids.

16. SECURITY CLASSIFICATION OF:			17. LIMITATION OF ABSTRACT	18. NUMBER OF PAGES	19a. NAME OF RESPONSIBLE PERSON
a. REPORT	b. ABSTRACT	c. THIS PAGE			Matthew Shawkey
U	U	U	UU	51	19b. TELEPHONE NUMBER *(Include area code)* 330-907-3686

Reset

Final Technical Report

AFOSR FA9550-13-1-0222

CHARACTERIZATION AND BIOMIMCRY OF AVIAN NANOSTRUCTURED TISSUES

Dr. Matthew D. Shawkey, Department of Biology Integrated Bioscience Program,
University of Akron, OH 44325-3908 (shawkey@uakron.edu)

Table of contents

Abstract

Understanding the properties and development of complex morphological traits may spark advances in the biomimetic design of new self-assembling multifunctional materials. Thus, we are using cutting-edge techniques to (I) identify previously unexplored chemical and physical properties of, and (II) synthetically mimic, color-producing nanostructures built from keratin and melanin in bird feathers.

For (I) we are testing four properties of optical nanostructures: (1) Refractive index and chemistry. We use plasmonics to measure refractive index of melanins and synchrotron-based Vacuum Ultraviolet Laser Desorption Mass Spectrometry techniques to compare their chemistry. We have optimized techniques for measurement of refractive index and have made significant progress understanding the chemistry that contributes to variation in color of feathers**.** (2) Tensile strength. We use atomic force microscopy to quantify how both the morphology and chemistry of individual melanosomes, as well as their organization into nanostructures, affects their material properties. We have a full dataset on tensile strength of iridescent barbules, and are currently collecting one on non-iridescent barbules for comparison (3) Thermoregulation. We use Fourier transform Infrared Spectroscopy and infrared imaging techniques to test how the wavelength selectivity caused by the organization of melanosomes into nanostructures affects absorbance. (4) Hydrophobicity. We use contact angle goniometry and modeling to determine how macrostructural modifications associated with nanostructures may affect hydrophobicity and directional water movement on feathers. We have identified nanostructured surfaces that create bright white color and superhydrophobicity.

For part (II) we use biomimetic approaches to elucidate the mechanisms by which these nanostructures self assemble. First, we replicate the depletion attraction forces that cause melanosomes to self assemble into iridescent nanostructures through a series of experiments in which we vary the conditions of polymerization of keratin and melanin blends. We have succeeded in organizing melanin particles into simple nanostructures, and are proceeding with experiments using blends and modified particle types. Second, we replicate the phase separation processes that cause self-assembly of non-iridescent nanostructures by producing keratin films from both nanostructured and unstructured keratin under varying conditions, and will identify differences in primary sequence or phosphorylation state between nanostructured and unstructured keratin. The results of this research will enhance our understanding of the multifunctionality of nanostructured traits and identify new means and natural materials for their production.

Vertebrate animal disclaimer

All feather samples were obtained either from study skins of dead birds housed in museums or from collaborators. Thus, no protocol for use of vertebrate animals is needed.

Progress on objective I:

1) Manakins produce bright iridescent feather colors without melanosomes.

Branislav Igic, Liliana D'Alba, Matthew D. Shawkey

Abstract

Males of many species often use colourful and conspicuous ornaments to attract females. Among these, male manakins (family: Pipridae) provide classic examples of sexual selection favouring the evolution of bright and colourful plumage coloration. The highly iridescent feather colours of birds are most commonly produced by the periodic arrangement of melanin-containing organelles (melanosomes) within a β-keratin matrix. Melanin increases the saturation of iridescent colours seen from optimal viewing angles by absorbing back-scattered light to, but at the same time this may reduce wide-angle brightness of these signals, contributing to a dark background appearance. We examined the nanostructure of four manakin species (*Lepidothrix isidorei*, *L. iris*, *L. nattereri*, and *L. coeruleocapilla*) to identify how they produce their bright plumage colours. Feather barbs of all four species were characterised by dense and fibrous internal spongy matrices that likely increase scattering of light within the barb. The iridescent, yet whitish, colours of *L. iris* and *L. nattereri* feathers were not produced by periodically arranged melanosomes within barbules, but by periodic matrices of air and β-keratin within barbs. *L. iris* crown feathers were able to produce a dazzling display of colours with small shifts in viewing geometry, likely due to their periodic nanostructure, flattened barb morphology, and disorder at a microstructural level. We hypothesize that iridescent plumage ornaments of male *L. iris* and *L. nattereri* are under selection to increase brightness or luminance across wide viewing angles, which may potentially increase their detectability by females during dynamic and fast-paced courtship displays in a dim environment.

Keywords: Animal coloration, inverse-opal, iridescence, *Lepidothrix*, manakin, ultra-white

Introduction

Coloration has diverse functions and can communicate information such as an individual's quality, aggression, genetic make-up, or toxicity (Ruxton et al., 2004; Pryke and Griffith, 2009; Shi et al., 2015; Young et al., In Press). Sexual selection is the primary evolutionary driver of ornamentation among animals and has produced some of the most extraordinary colours among animals (Kirkpatrick and Ryan, 1991; Price et al., 1993; Andersson, 1994). Evolution of conspicuous and elaborate colour patterns is often driven by mate-choice or intra-sexual competition for mates (Doucet et al., 2007; Chen et al., 2012), but also aposematic and warning communication (Ruxton et al., 2004; Kraemer et al., 2015). Indeed, males of diverse taxa use colourful traits to attract females, including spiders, birds, fishes, reptiles, and mammals (Kodric-Brown, 1985; Setchell and Jean Wickings, 2005; Stuart-Fox and Moussalli, 2008; Girard and Endler, 2014). Sexual selection often favours conspicuous colours, which can be achieved by maximizing their chromatic or achromatic contrast against the environment (Endler, 1992; Uy and Endler, 2004; Doucet et al., 2007).

Colouration of animals is produced by pigments, nanostructures, or a combination of both pigments and nanostructures (Shawkey and Hill, 2006; Bagnara et al., 2007; Kinoshita, 2008; Stavenga et al., 2011; D'Alba et al., 2012). Pigments produce colour by selectively absorbing specific wavelengths of visible light while allowing others to be reflected. By contrast, structural colours are produced by periodic nanostructures that interfere with light within visible wavelengths and cause particular wavelengths to be amplified or attenuated through constructive and destructive interference, respectively (Vukusic and Sambles, 2003; Kinoshita, 2008). Although not traditionally defined as a colour, white is a common and important component of animal colouration and is produced by the diffuse and wavelength-independent scattering of light by disordered nanostructures (Dyck, 1979; Vukusic et al., 2007) and is involved in the perception of luminance or brightness of colour signals. Unlike pigments, structural colours are capable of producing colours that change with viewing geometry (iridescence; Osorio and Ham, 2002; Kinoshita, 2008; Doucet and Meadows, 2009). Iridescence is a common and important component of avian courtship displays (Hill, 2006), and males of many species use dazzling displays of changing colours to impress or capture the attention of females (e.g. *Parotia lawesii and Pavo cristatus*; Stavenga et al., 2010; Dakin and Montgomerie, 2013).

The iridescent plumage coloration of birds described so far requires the presence and nanoscale arrangement of melanosomes (melanin-containing organelles) to produce visible colour. Melanins are pigments that can absorb light across all wavelengths visible to animals (300-700 nm; Meng and Kaxiras, 2008). However, for many birds, the precise arrangement of melanosomes within their feather barbules produces iridescent colours by causing particular reflected wavelengths to be amplified while others are attenuated as light travels through materials that periodically vary in refractive index (i.e. air, β-keratin, and melanin; Greenewalt et al., 1960; Stavenga et al., 2010; Maia et al., 2011; Eliason et al., 2013). Independently of nanoscale arrangement of melanosomes, some species produce weakly iridescent colours through quasi-ordered nanostructures of β-keratin and air within feathers barbules or barbs respectively (Noh et al., 2010a). However, ,this iridescence is not visible under natural light conditions (Osorio and Ham, 2002; Noh et al., 2010a). A previous report suggested that back-billed magpies produce iridescent color through an ordered matrix of keratin and air (Vigneron et al. 2006). However, the morphology of this matrix is highly similar to previously described arrays of hollow melanosomes that produce iridescen color, suggesting that additional research is needed to confirm its nature. Although the β-keratin cortex of feather barbs can produce weak iridescence through thin-film interference without the contribution of melanosomes, this effect is only important at micro-scales and likely

contributes minimally to the coloration seen at visually relevant spatial scales (Stavenga et al., 2011).

Strong directional reflection of colour is a common property of many strongly iridescent feathers.. For example, the spectacular iridescent patches of many species (e.g. hummingbirds, ribbon-tailed astrapias *Astrapia mayeri*, and magnificent riflebirds *Ptiloris magnificus*) reflect bright, saturated, and iridescent colours in specific directions (often in specular or mirror-like directions), while appearing dark or cryptic at other angles or diffusely (Osorio and Ham, 2002; Doucet and Meadows, 2009). This directional reflection of colour is due to a planar morphology of colour-producing barbules that reflects light in a particular direction (e.g. the flat or boomerang shaped barbules in P. lawesii; Stavenga et al., 2010; Stavenga et al., 2015). By contrast, a curved barbule morphology reduces both the magnitude of colour change and the angle-dependence of iridescent feather colours, so that colour can be seen from a larger range of viewing angles (Dyck, 1987; Yoshioka and Kinoshita, 2002). Melanosomes also likely play an important role in increasing the directionality of highly iridescent feathers. By absorbing light that is diffusely scattered or reflected, melanosomes increase the saturation of iridescent feather colours (Yoshioka and Kinoshita, 2002; Shawkey and Hill, 2006) and contribute to their dark background appearance as suggested by Brink and Van Der Berg (2004). In turn, this may explain the rarity of iridescent feathers with a light background appearance.

Male manakins (family: Pipridae) use some of the brightest plumage colours among birds to attract females (Kirwan and Green, 2011). Manakins are a diverse clade of small frugivorous birds that contains 42-57 species (depending on taxonomic classification) distributed across the Neotropics (Prum, 1990; Rêgo et al., 2007; Ohlson et al., 2013). Males of most species court females within leks using elaborate colours, strange and unique sounds, and stereotyped movements (Prum, 1990; Endler and Thery, 1996; Prum, 1998; Durães, 2009; Kirwan and Green, 2011; Lukianchuk and Doucet, 2014). Males in the genus *Lepidothrix* display exceptionally bright colours on their crown and rump feathers (figure 1), such as ultra-whites, vibrant blues, golds, and iridescent opal-like colours (Kirwan and Green, 2011; this study). Despite considerable interest in the function and evolution of coloration within this family of birds (Endler and Thery, 1996; Doucet et al., 2007; Ribeiro et al., 2015), characterization of their coloration and examinations of colour production mechanisms have primarily focussed on non-iridescent blues and greens (Saranathan et al., 2012). Here, we examined and compared the coloration and colour production mechanisms across plumage ornaments of four *Lepidothrix* species, primarily focussing on two species with iridescent plumage but, unusually, white or pale coloured background appearance.

Methods

We examined the vibrant crown and rump feather colours of four different *Lepidothrix* manakins (figure 1): ultra-white crown feathers of the blue-rumped manakin (*L. isidorei*); opalescent crown feathers of the opal-crowned manakin (*L. iris*); pinkish-white rump feathers of the snow-capped manakin (*L. nattereri*); and blue rump feathers of the cerulean-capped manakin (*L. coeruleocapilla*). All feathers were kindly provided by the Field Museum of Natural History (Chicago, IL).

Reflectance Measurements

We measured specular and diffuse spectral reflectance of feathers between 300 and 700 nm. For each measurement, we flattened single feathers by taping their calamus to low reflective black velvet fabric and oriented the feathers such that the incident light beam hit the pennacous barbs at a proximal to distal orientation. We measured specular reflectance between 10° and 50° from coincident normal at 5° increments at two different locations per

feather using a spectrometer equipped with two fibres that rotate independently from one another; one fibre was connected to a light source (AvaLight-XE pulsed xenon light, Avantes Inc., Broomfield, CO, USA) and the other fibre to a spectrometer (AvaSpec-2048 spectrometer). We measured specular reflectance at coincident normal and back-scattering at 45° using a bifurcated probe and a block holder (AFH-15), and measured diffuse reflectance collectively across all possible angles at three different locations per feather using an integrating sphere with a black gloss trap to exclude specular reflectance (AvaSphere-50-REFL). To examine the scattering processes responsible for producing the different reflectance peaks, we used Glan-Thompson linear polarizers (Harrick Scientific Products, Pleasantville, NY, USA) to identify whether reflected light was either parallel (co-polarization) or perpendicular (cross-polarization) to that of polarized incident light (Noh et al., 2010a; Noh et al., 2010b). Light that is scattered only once will maintain co-polarization, whereas a multiple scattering process would lead to cross-polarization (Noh et al., 2010a; Noh et al., 2010b). All reflectance measurements were taken relative to a diffuse white standard (WS-2, Avantes).

Examination of feather structure

To identify the mechanisms of colour production, we examined the structure of whole feathers and feather barbs using light, scanning electron, and transmission electron microscopes. We primarily focussed our attention on the structure of barbs, rather than barbules, because barbules were either absent from colour producing regions or greatly reduced in size and fused to the underside of barbs across species (figure1; see Results). For light microscopy, we used a *Leica S8AP0* (Leica Microsystems, Germany) equipped with a MicroPublisher 5.0 RTV FireWire camera (Q Imaging, Canada). To prepare samples for scanning electron microscopy (SEM), we fragmented barbs using a scalpel, and mounted them onto aluminium stubs to allow visualisation of cross-sections, which we then coated with gold/palladium for 3 min (Igic et al., 2015). We also mounted 1 µm thick barb cross and transverse sections (embedded in Epon and sectioned using protocol described below) to allow SEM visualisation of nanostructure across a flatter plane. We imaged barb sections using a JSM-7401F SEM (JEOL, Japan), at a working distance of 7mm, and an accelerating voltage of 7 kV. To prepare samples for transmission electron microscopy (TEM), we first washed fragmented barbs in 100% ethanol for 20 min twice, and then immersed the washed fragments in successive concentrations of 15, 50, 70, and 100% Epon (diluted using 100% ethanol) for 24 hours (Shawkey et al., 2003). Barbs were then placed in moulds to allow sectioning of both cross- and transverse-sections and were cured in an incubator for 24 hours at 60°C. We cut 100 nm thick sections using an Ultra 45 diamond knife (Diatome Ltd, Biel, Switzerland) on a Leica EM UC6 ultramicrotome (Leica Microsystems GmbH, Germany), which we placed on 200 mesh, formvar-coated copper grids (EMS, USA) and imaged using a JEOL JEM-1230 TEM operating at 120 kV. We examined the spatial ordering of the barb nanostructure using the Fast Fourier Transform (FFT) tool in ImageJ (http://imagej.nih.gov/ij/). We acknowledge the limitations of using TEM images and 2D FFT to test assumptions about the 3D structures of biological nanostructures (Shawkey et al., 2009; 2012), and therefore use this only as an exploratory tool to examine the potential for nanostructural periodicity.

Optical Modelling

The internal nanostructures of *L. iris* and *L. nattereri* barbs resembled those of hexagonally-packed inverse opals. Therefore, we used a modified equation based on Bragg's and Snell's laws (Eq 1) to estimate the peak wavelength of reflectance produced by a close-packed hexagonal nanostructure (Aguirre et al., 2010),

$$\lambda_{max} = 1.633D\sqrt{n_{eff}^2 - sin^2\theta} \quad \text{(Eq 1.)}$$

where λ_{max} is wavelength with maximum reflectance, D is the average void spacing, n_{eff} is the effective refractive index of the material, and θ is the angle of specular reflection. For D, we used the average distance between void centroids (257 nm ± 3.9 s.e and 307 nm ± 3.9 s.e. for *L. iris* and *L. nattereri*, respectively), which we measured as an average nearest neighbour distance between centroids of 58-69 voids on TEM images (149-162 individual nearest neighbour distances). The effective refractive index can be calculated using Eq. 2

$$n_{eff} = \varphi n_{voids} + (1 - \varphi)n_{walls} \quad \text{(Eq 2.)}$$

where φ is the solid fraction of the material, and n_{voids} and n_{walls} are the respective refractive indices of the spherical voids and the solid walls of the material. We estimated φ using the binary function of ImageJ to calculate the relative proportions walls relative to voids on a section of the barb on TEM images. Excluding the cortex and the cell vacuoles, the solid walls contributed to approx. 72% of the barbs internal structure for both *L. iris* and *L. nattereri*. For the refractive indices of the voids and the solid walls, we respectively used the refractive index of air (n = 1) and β-keratin (n = 1.56). Although this simple theory can estimate the wavelength of peak reflectance of isotropic hexagonally close-packed nanostructures, it cannot be used to estimate any other spectral characteristics of materials and cannot take into account the curvature and cortex thickness of barbs, nor the variability in the nanostructure (table S1), all of which could affect the spectral properties of these feathers.

In addition to the equations for a hexagonally close-packed structure, we used optical equations published in Xiao et al. (2014) to test how well the predictions of 1D multilayer structure fit the measured spectra for *L. iris* and *L. nattereri*. These calculations were based on cortex thicknesses of 518 and 740 nm (table S1), air layer thicknesses of 146 and 250 nm, keratin layer thicknesses or 104 and 98 nm (all respectively for *L. iris* and *L. nattereri*); 15 layer stacks, which was the approximate number of keratin/air layers between the edge and centre of medullary cells; volume fractions of 72% for the air layer; and the above specified refractive indices for air and β-keratin.

Results

Almost all the manakin feathers examined here displayed angle-dependent specular coloration and broad diffuse reflectance (figures 3 and S1). *L. iris* crown feathers and *L. nattereri* rump feathers appeared iridescent to the human eye (figure 1 and video S1), and their spectra showed peaks that shifted to narrower wavelengths with increasing angles of specular reflection (figure 3) but uniform reflectance across integrated diffuse angles (figure S1). By contrast, *L. isidorei* crown feathers had broad reflectance at both specular and diffuse geometries, whereas the *L. coeruleocapilla* rump feathers had blue and UV peaks in both specular and diffuse reflectance geometries (figures 2 and S1). Both the *L. iris* crown feathers and *L. nattereri* rump feathers had secondary peaks at shorter wavelengths, which unlike their primary peaks lost their polarization (peaks were present in both co- and cross-polarization), suggesting that they were produced either by higher-order scattering or diffraction (figures S2 and S3; Noh et al., 2010b). As a result, the *L. iris* crown feathers displayed dramatic colour changes (can we say this more quantitatively? mention change in nm?) with subtle changes in viewing geometry, appearing yellowish-green at specular geometries, while blue or purple at non-specular geometries (figure 3 and video S1).

The bright coloration of these manakins' feathers was associated with dense internal barb nanostructures, absence or limited distribution of light absorbing melanosomes, and a

flattened barb morphology for *L. iris* feathers (figures 4, 5, and S4). The white barbs of *L. isidorei* and *L. nattereri* lacked barbules at their distal ends, whereas *L. coeruleocapilla* and *L. iris* barbs contained short, flat, and melanised barbules at the distal ends (figures 4, 5, and S4). Barbs of all species were comprised of medullary cells, which contained central air-filled vacuoles and dense spongy networks of β-keratin at their exteriors, conforming to the sphere-type category for feather barb nanostructure (figure 5; Prum, 2006; Saranathan et al., 2012). The central air-filled vacuoles comprised a larger portion of *L. isidorei* crown feather barbs compared with the other species examined here (table S1). *L. isidorei* and *L. nattereri* barbs lacked melanosomes, whereas *L. iris* feathers had a restricted distribution of melanosomes along one edge of their barbs (figures 4, 5, and S4). *L. coeruleocapilla* feathers had a broad distribution of melanosomes within their barbs and barbules (figures 5 and S4).

The level of spatial ordering of their internal nanostructures (figures 5 and S5) varied between the four manakin species. *L. iris* barb nanostructures were most ordered with a hexagonally packed structure characteristic of inverse opal materials but lacking long-range order (figures 5 and S5). *L. nattereri* and *L. coeruleocapilla* barbs had similar structures near their barb cortex but with lower spatial order relative to *L. iris* barbs (figures 5 and S5). The *L. isidorei* barbs showed the least spatial ordering among the species examined (figures 5 and S5). The diameter of voids differed across the four species, and none of the species had perfectly spherical or identically-sized voids (table S1), indicating that none of the feathers had an isotropic nanostructure. Despite their apparent absence of long-range order (figure S5), the peak reflectance predicted by optical calculations for 3D inverse-opal like structures matched the measured peak reflectance for both *L. iris* and *L. nattereri* feathers, and better than optical calculations for a 1D multi-layer structure (figure 6). Removing the barbules did not visibly affect the coloration of *L. iris* feathers, whereas crushing the barb structure caused their barbs to become translucent, confirming the structural origin of the coloration (figure S6).

Discussion

The conspicuous and bright plumage colours of four *Lepidothrix* manakins were associated with dense and fibrous internal barb nanostructures. The four species studied here differed in overall barb shape, the degree of periodicity and distance between periodic structures within the barb's internal spongy β-keratin matrix, and the presence and distribution of melanosomes. The dense internal networks of β-keratin and air create many interfaces for light scattering, which in turn would increase the overall brightness (the total broad reflectance across all visible wavelengths) of these plumage patches across all angles (Dyck, 1979; Hanrahan and Krueger, 1993; Shawkey and Hill, 2005). The internal nanostructure of *L. iris* barbs is similar to barbs of several for other species, including other manakins (this study; Saranathan et al., 2012), but differed by being more periodic. This periodicity, in combination with a flat barb morphology and limited presence of melanosomes, produced highly directional and strongly iridescent coloration on a pale background for *L. iris* feathers.

Although we detected angle dependent colour changes for three of the four manakin species, only *L. iris*, and possibly also *L. nattereri*, are iridescent under natural light conditions (functionally iridescent). Structural blue colours produced by a quasi-ordered nanostructure, similar to that of *L. coeruleocapilla*, can show iridescence under the directional light of a spectrometer, but not under natural light conditions, due to the isotropic nature of the spongy matrix and the prevalence of back-scattered light (Osorio and Ham, 2002; Noh et al., 2010a). Although the periodicity of *L. nattereri* barbs was similar to that of *L. coeruleocapilla*, reddish and iridescent highlights can be seen on the feathers by human vision at particular angles, and therefore also possibly by female manakins under natural light conditions. Interestingly, *L. nattereri* rump feathers have been described as brilliant white

without reference to their iridescence (Kirwan and Green, 2011), suggesting possibly that there may be subtle geographic or sub-species variation in their coloration. Alternatively, the absence of barbules to structure *L. nattereri* barbs into a uniform plane and a rounded barb morphology may reduce or mask the presence of these highlights when observing these plumage patches as a whole. Therefore, the presence of iridescence in this species requires further investigation. By contrast, the pure ultra-white coloration of *L. isidorei* crown feathers is associated with a dense and disorganized internal nanostructure that likely causes wavelength-independent scattering of light to dominate (e.g. Vukusic et al., 2007).

The *L. iris* crown feathers were particularly dazzling and produced diverse colours with small changes in viewing geometry independently of melanosome arrangement (video S1). To our knowledge, they provide the first reported examples of feathers with highly directional iridescence without melanosomes. Depending on angle of observation, *L. iris* crown feathers can appear white, yellowish-green, blue or purple. These angle-dependent colour changes are associated with a combination of short-range hexagonal nanostructural periodicity, a flattened barb shape, long-range disorder imposed by the presence of vacuoles at the centre medullary cells, and restricted distribution of melanosomes. For example, the yellowish-green colour arises through diffraction of light by the periodically arranged air and β-keratin matrix and is likely further enhanced in the specular direction by a flattened barb morphology. By contrast, blues and purples are perceived at non-specular angles, and therefore likely arise from either from higher order diffraction (e.g. Eliason et al., 2013) or multiple scattering from a quasi-ordered nanostructure (e.g. Noh et al., 2010a). Light scatterometry, Small-angle X-ray scattering, and finite-difference time-domain modelling (Saranathan et al., 2012; Wilts et al., 2014) are necessary to further clarify the exact production mechanisms for colours observed at non-specular angles.

Not using melanosomes to produce iridescent plumage may potentially trade-off more saturated angle-dependent colours for an iridescent signal that remains visible across a wider range of angles. For example, including carbon black as a light absorbing agent within structural coloured films of colloidal particles increases their colour saturation through absorption of multiply scattered light, at the expense of reduced total reflectance over human visible wavelengths (Takeoka et al., 2013; Ohtsuka et al., 2015). The absence of melanosomes (and hence washing out of color due to increased multiple scattering) may further explain why the *L. nattereri* rump feathers appear pinkish, rather than a saturated red like structural reds produced using melanosomes (e.g. Greenewalt et al., 1960; Eliason et al., 2013; Xiao et al., 2014). *L. nattereri* rump feathers may appear purple or pink, rather than red, if on a darker melanised background (Magkiriadou et al., 2014) because they lack long-range order in their nanostructure and exhibit secondary peaks at shorter wavelengths. Although *L. iris* barbs contained flat melanised barbules on their posterior side, and a restricted distribution of melanosomes within the barb cortex, these melanosomes appeared to contribute little to barb colour production as coloration persisted on unmelanised regions of barbs even after removal of the barbules. The limited posterior distribution of melanosomes on *L. iris* barbs may absorb some of the backscattered light and increase purity of colours to some extent (Shawkey and Hill, 2006). The higher refractive index contrast between β-keratin and air (1.56 vs 1) than between β-keratin and melanosomes (1.56 vs. 1.7; Leertouwer et al., 2011; Stavenga et al., 2015) may also increase the scattering of light within the nanostructure and may contribute to a paler appearance; however, this hypothesis requires further investigation.

Our findings suggest that the plumage ornaments of some *Lepidothrix* manakins are under selection to maximise their brightness across all possible viewing geometries, resulting in iridescent colour signals with a pale background. Increasing the total reflectance across all visible wavelengths (achromaticity) and viewing angles may increase the detectability of

these traits by females as males fly around in dim forest light conditions. Birds, like most animals, process achromatic and chromatic components of colour signals differently, and achromatic components are particularly important in detection of motion, form, and patterns (Osorio and Vorobyev, 2005; Kemp et al., 2015), and therefore could be more important during the dynamic and fast-paced aspects of a male manakin's display. Although the courtship displays of the species examined here are not well described, their displays can involve extremely quick flights between several locations (Anciães, 2014). *Lepidothrix* manakins reside within neotropical rainforests where tall and dense trees restrict the amount of sunlight transmitted through the forest canopy (Doucet et al., 2007), and species generally benefit from being brighter in darker environments (Marchetti, 1993). Ambient light is an important factor in avian courtship rituals including those of manakins: male manakins are known to select display sites with more available light or to manipulate the environment to increase the amount of available light (Endler and Thery, 1996; Uy and Endler, 2004). Intriguingly, the iridescent plumage patches of both *L. iris* and *L. nattereri* showed primary peaks at longer wavelengths which may be particularly important in luminance perception (Osorio and Vorobyev, 2005). Crown feathers of *L. iris* in particular are able to produce abrupt flashes of bright colour, which may be particularly dazzling as a male tilts his head during specific stages of display (e.g. Anciães, 2014). Therefore, both the achromatic and chromatic components of male plumage ornaments are important in display.

It is unclear why these types of pale opalescent colours are not more common among birds. Although several other species are described as having opalescent plumage (*Tangara callophrys* and *T. velia*), it is yet unclear whether these species possesses similar spectral properties or production mechanisms as manakins described here. These ordered nanostructures within barbs may be physiologically more difficult to produce than melanosome-based iridescent colours within barbules. For example, these highly periodic arrangements of β-keratin and air may be difficult to achieve through the passive self-assembly processes of phase separation likely used to produce the quasi-ordered nanostructures of some feather barbs (Saranathan et al., 2012), and this hypothesis should be tested. Furthermore, to better understand the function of these types of ornaments, future work should examine how these colour patches appear to a female in relation to natural light conditions and the male's movements during display.

Figure captions

Figure 1. Study species and feathers. Photographs of (a) *L. isidorei* (credit Ben Sadd) and (b) *L. iris* (credit Marcelo Barreiros), as well as (c) *L. isidorei* crown, (d) *L. iris* crown, (e) *L. nattereri* rump, and (f) *L. coeruleocapilla* rump feathers. Scale bars: 0.5 mm.

Figure 2 Specular reflectance of individual feathers at 5° angle increments starting at 10° (dark grey), and up to 50° (light gray), from coincident normal (0°): (a) *L. isidorei* crown, (b) *L. iris* crown, (c) *L. nattereri* rump, and (d) *L. coeruleocapilla* rump feathers. Due to small size, crown feathers could only be measured up to 45° from coincident normal.

Figure 3. *L. iris* crown feathers at incident light at different viewing geometries: (a & c) normal incidence; (b & d) 45° + 30° from normal incidence; (e) in transmittance. Images show feathers either dorsal side up (a & b) or ventral side up (c-d). Black regions seen in (c-d) are melanised barbules and narrow melanised region of the barb cortex. Scale bars are 0.5 mm (a & b) and 0.1 mm (c-d).

Figure 4. SEM images of whole barb cross-sections for (a) *L. isidorei* crown, (b) *L. iris* crown, (c) *L. nattereri* rump, and (d) *L. coeruleocapilla* rump feathers. Melanised regions of barbs are indicated by dashed lines and the melanised barbule with "B". Scale bars: 10 μm.

Figure 5. SEM images of barb cross-sections at the junction of the cortex and medulla for (a) *L. isidorei* crown, (b) *L. iris* crown, (c) *L. nattereri* rump, and (d) *L. coeruleocapilla* rump feathers. Melanised barbule is indicated with "B". Scale bars: 1 μm.

Figure 6. Measured (black lines) and predicted spectral properties predicted using optical models for 3D inverse-opal photonic crystals (blue lines) or 1D multilayers (red lines) for *L. iris* crown (a & b) and *L. nattereri* rump (c & d) feathers at normal incidence (a & c) or across different specular angles (b & d). Note that (c) illustrates the predicted secondary reflectance peak for a 1D multilayer, whereas values in (d) are peak reflectance for the primary peak.

References

Aguirre CI, Reguera E, Stein A, 2010. Tunable colors in opals and inverse opal photonic crystals. Adv Funct Mater 20:2565-2578. doi: 10.1002/adfm.201000143.

Anciães M, 2014. Opal-crowned Manakin (*Lepidothrix iris*) YouTube.com.

Andersson M, 1994. Sexual Selection. Princeton, NJ: Princeton Univ. Press.

Bagnara JT, Fernandez PJ, Fujii R, 2007. On the blue coloration of vertebrates. Pigm Cell Res 20:14-26. doi: 10.1111/j.1600-0749.2006.00360.x.

Brink D, Van Der Berg N, 2004. Structural colours from the feathers of the bird *Bostrychia hagedash*. Journal of Physics D: Applied Physics 37:813-818. doi: 10.1088/0022-3727/37/5/025.

Chen I, Stuart-Fox D, Hugall AF, Symonds MR, 2012. Sexual selection and the evolution of complex color patterns in dragon lizards. Evolution 66:3605-3614. doi: 10.1111/j.1558-5646.2012.01698.x.

D'Alba L, Kieffer L, Shawkey MD, 2012. Relative contributions of pigments and biophotonic nanostructures to natural color production: a case study in budgerigar (*Melopsittacus undulatus*) feathers. J Exp Biol 215:1272-1277. doi: 10.1242/jeb.064907

Dakin R, Montgomerie R, 2013. Eye for an eyespot: how iridescent plumage ocelli influence peacock mating success. Behavioral Ecology 24:1048-1057. doi: 10.1093/beheco/art045.

Doucet SM, Meadows MG, 2009. Iridescence: a functional perspective. J R Soc Interface 6:S115-S132. doi: 10.1098/rsif.2008.0395.focus.

Doucet SM, Mennill DJ, Hill GE, 2007. The evolution of signal design in manakin plumage ornaments. Am Nat 169:S62-S80. doi: 10.1086/510162.

Durães R, 2009. Lek structure and male display repertoire of blue-crowned manakins in eastern Ecuador. The Condor 111:453-461. doi: 10.1525/cond.2009.080100.

Dyck J, 1979. Winter plumage of the rock ptarmigan: structure of the air-filled barbules and function of the white colour. Dansk Orn Foren Tidsskr 73:41-58.

Dyck J, 1987. Structure and light reflection of green feathers of fruit doves (*Ptilinopus* spp.) and an imperial pigeon (*Ducula concinna*). Biol Skr:1-43.

Eliason CM, Bitton P-P, Shawkey MD, 2013. How hollow melanosomes affect iridescent colour production in birds. Proc Roy Soc B 280:20131505. doi: 10.1098/rspb.2013.1505.

Endler JA, 1992. Signals, signal conditions, and the direction of evolution. Am Nat:S125-S153. doi: 10.1086/285308.

Endler JA, Thery M, 1996. Interacting effects of lek placement, display behavior, ambient light, and color patterns in three neotropical forest-dwelling birds. Am Nat:421-452. doi: 10.1086/285934.

Girard MB, Endler JA, 2014. Peacock spiders. Curr Biol 24:R588-R590. doi: 10.1016/j.cub.2014.05.026.
Greenewalt CH, Brandt W, Friel DD, 1960. The iridescent colors of hummingbird feathers. Proc Am Philos Soc:249-253. doi: doi:10.1364/JOSA.50.001005.
Hanrahan P, Krueger W, 1993. Reflection from layered surfaces due to subsurface scattering. Proceedings of the 20th annual conference on Computer graphics and interactive techniques:165-174.
Hill GE, 2006. Female mate choice for ornamental coloration. In: Hill GE, McGraw KJ, editors. Bird Coloration: Function and Evolution Cambridge, MA: Harvard University Press. p. 137-200.
Igic B, Fecheyr-Lippens D, Xiao M, Chan A, Hanley D, Brennan PRL, Grim T, Waterhouse GIN, Hauber ME, Shawkey MD, 2015. A nanostructural basis for gloss of avian eggshells. J R Soc Interface 12. doi: 10.1098/rsif.2014.1210.
Kemp DJ, Herberstein ME, Fleishman LJ, Endler JA, Bennett ATD, Dyer AG, Hart NS, Marshall J, Whiting MJ, 2015. An integrative framework for the appraisal of coloration in nature. Am Nat 185:705-724. doi: 10.1086/681021.
Kinoshita S, 2008. Structural Colors in the Realm of Nature. Singapore: World Scientific.
Kirkpatrick M, Ryan MJ, 1991. The evolution of mating preferences and the paradox of the lek. Nature 350:33-38. doi: 10.1038/350033a0.
Kirwan GM, Green G, 2011. Cotingas and Manakins. Princeton, NJ: Princeton University Press.
Kodric-Brown A, 1985. Female preference and sexual selection for male coloration in the guppy (*Poecilia reticulata*). Behav Ecol Sociobiol 17:199-205. doi: 10.1007/BF00300137.
Kraemer AC, Serb JM, Adams DC, 2015. Batesian mimics influence the evolution of conspicuousness in an aposematic salamander. Journal of Evolutionary Biology. doi: 10.1111/jeb.12622.
Leertouwer HL, Wilts BD, Stavenga DG, 2011. Refractive index and dispersion of butterfly chitin and bird keratin measured by polarizing interference microscopy. Opt Express 19:24061-24066. doi: 10.1364/OE.19.024061.
Lukianchuk K, Doucet S, 2014. Cooperative courtship display in long-tailed manakins chiroxiphia linearis: predictors of courtship success revealed through full characterization of display. J Ornithol 155:729-743. doi: 10.1007/s10336-014-1059-3.
Magkiriadou S, Park J-G, Kim Y-S, Manoharan VN, 2014. Absence of red structural color in photonic glasses, bird feathers, and certain beetles. Phys Rev E 90:062302. doi: 10.1103/PhysRevE.90.062302.
Maia R, D'Alba L, Shawkey MD, 2011. What makes a feather shine? A nanostructural basis for glossy black colours in feathers. Proc Roy Soc B 278:1973-1980. doi: 10.1098/rspb.2010.1637.
Marchetti K, 1993. Dark habitats and bright birds illustrate the role of the environment in species divergence. Nature 362:149-152. doi: 10.1038/362149a0.
Meng S, Kaxiras E, 2008. Theoretical models of eumelanin protomolecules and their optical properties. Biophys J 94:2095-2105. doi: 10.1529/biophysj.107.121087.
Noh H, Liew SF, Saranathan V, Mochrie SG, Prum RO, Dufresne ER, Cao H, 2010a. How noniridescent colors are generated by quasi-ordered structures of bird feathers. Adv Mater 22:2871-2880. doi: 10.1002/adma.200903699.
Noh H, Liew SF, Saranathan V, Prum RO, Mochrie SG, Dufresne ER, Cao H, 2010b. Double scattering of light from biophotonic nanostructures with short-range order. Opt Express 18:11942-11948. doi: 10.1364/OE.18.011942.

Ohlson JI, Fjeldså J, Ericson PG, 2013. Molecular phylogeny of the manakins (Aves: Passeriformes: Pipridae), with a new classification and the description of a new genus. Mol Phylogenet Evol 69:796-804. doi: 10.1016/j.ympev.2013.06.024.

Ohtsuka Y, Seki T, Takeoka Y, 2015. Thermally Tunable Hydrogels Displaying Angle-Independent Structural Colors. Angew Chem Int Edit 127:1521-3757. doi: 10.1002/ange.201507503.

Osorio D, Ham A, 2002. Spectral reflectance and directional properties of structural coloration in bird plumage. J Exp Biol 205:2017-2027.

Osorio D, Vorobyev M, 2005. Photoreceptor sectral sensitivities in terrestrial animals: adaptations for luminance and colour vision. Proc Roy Soc B 272:1745-1752. doi: 10.1098/rspb.2005.3156.

Price T, Schluter D, Heckman NE, 1993. Sexual selection when the female directly benefits. Biol J Linn Soc 48:187-211. doi: 10.1111/j.1095-8312.1993.tb00887.x.

Prum R, 2006. Anatomy, physics, and evolution of structural colors. In: Hill GE, McGraw KJ, editors. Bird Coloration: Mechanisms and Measurements Cambridge, MA: Harvard University Press. p. 295-353.

Prum RO, 1990. Phylogenetic analysis of the evolution of display behavior in the Neotropical manakins (Aves: Pipridae). Ethology 84:202-231. doi: 10.1111/j.1439-0310.1990.tb00798.x.

Prum RO, 1998. Sexual selection and the evolution of mechanical sound production in manakins (Aves: Pipridae). Animal Behaviour 55:977-994. doi: 10.1006/anbe.1997.0647.

Pryke SR, Griffith SC, 2009. Postzygotic genetic incompatibility between sympatric color morphs. Evolution 63:793-798. doi: 10.1111/j.1558-5646.2008.00584.x.

Rêgo PS, Araripe J, Marceliano ML, Sampaio I, Schneider H, 2007. Phylogenetic analyses of the genera *Pipra*, *Lepidothrix* and *Dixiphia* (Pipridae, Passeriformes) using partial cytochrome b and 16S mtDNA genes. Zool Scr 36:565-575. doi: 10.1111/j.1463-6409.2007.00301.x.

Ribeiro RD, McCormack JE, Álvarez HG, Carrasco L, Grether GF, Mena-Olmedo P, Sedano R, Smith TB, Karubian J, 2015. Loss of sexual dimorphism is associated with loss of lekking behavior in the green manakin *Xenopipo holochora*. J Avian Biol 46:307-314. doi: 10.1111/jav.00545.

Ruxton GD, Sherratt TN, Speed MP, 2004. Avoiding Attack: The Evolutionary Ecology of Crypsis, Warning Signals, and Mimicry. New York, NY: Oxford University Press.

Saranathan V, Forster JD, Noh H, Liew S-F, Mochrie SGJ, Cao H, Dufresne ER, Prum RO, 2012. Structure and optical function of amorphous photonic nanostructures from avian feather barbs: a comparative small angle X-ray scattering (SAXS) analysis of 230 bird species. J R Soc Interface. doi: 10.1098/rsif.2012.0191.

Setchell JM, Jean Wickings E, 2005. Dominance, status signals and coloration in male mandrills (*Mandrillus sphinx*). Ethology 111:25-50. doi: 10.1111/j.1439-0310.2004.01054.x.

Shawkey MD, Estes AM, Siefferman LM, Hill GE, 2003. Nanostructure predicts intraspecific variation in ultraviolet–blue plumage colour. Proc Roy Soc B 270:1455-1460. doi: 10.1098/rspb.2003.2390.

Shawkey MD, Hill GE, 2005. Carotenoids need structural colours to shine. Biology Letters 1:121-124. doi: 10.1098/rsbl.2004.0289

Shawkey MD, Hill GE, 2006. Significance of a basal melanin layer to production of non-iridescent structural plumage color: evidence from an amelanotic Steller's jay (*Cyanocitta stelleri*). J Exp Biol 209:1245-1250. doi: 10.1242/jeb.02115

Shawkey MD, Saranathan V, Pálsdóttir H, Crum J, Ellisman MH, Auer M, Prum RO, 2009. Electron tomography, three-dimensional Fourier analysis and colour prediction of a

three-dimensional amorphous biophotonic nanostructure. J R Soc Interface 6:S213-S220. doi: 10.1098/rsif.2008.0374.focus.

Shi NN, Tsai C-C, Camino F, Bernard GD, Yu N, Wehner R, 2015. Keeping cool: enhanced optical reflection and radiative heat dissipation in Saharan silver ants. Science 349:298-301. doi: 10.1126/science.aab3564.

Stavenga DG, Leertouwer HL, Marshall NJ, Osorio D, 2010. Dramatic colour changes in a bird of paradise caused by uniquely structured breast feather barbules. Proc Roy Soc B 278:2098–2104. doi: 10.1098/rspb.2010.2293.

Stavenga DG, Leertouwer HL, Osorio DC, Wilts BD, 2015. High refractive index of melanin in shiny occipital feathers of a bird of paradise. Light: Science & Applications 4:e243. doi: doi:10.1038/lsa.2015.16.

Stavenga DG, Tinbergen J, Leertouwer HL, Wilts BD, 2011. Kingfisher feathers–colouration by pigments, spongy nanostructures and thin films. J Exp Biol 214:3960-3967. doi: 10.1242/jeb.062620

Stuart-Fox D, Moussalli A, 2008. Selection for social signalling drives the evolution of chameleon colour change. PLoS Biol 6:e25. doi: 10.1371/journal.pbio.0060025.

Takeoka Y, Yoshioka S, Takano A, Arai S, Nueangnoraj K, Nishihara H, Teshima M, Ohtsuka Y, Seki T, 2013. Production of colored pigments with amorphous arrays of black and white colloidal particles. Angew Chem Int Edit 52:7261-7265. doi: 10.1002/anie.201301321.

Uy JAC, Endler JA, 2004. Modification of the visual background increases the conspicuousness of golden-collared manakin displays. Behavioral Ecology 15:1003-1010. doi: 10.1093/beheco/arh106.

Vigneron JP, Colomer J-F, Rassart M, Ingram AL, Lousse V, 2006. Structural origin of the colored reflections from the black-billed magpie feathers. Phys Rev E 73:021914. doi: 10.1103/PhysRevE.73.021914.

Vukusic P, Hallam B, Noyes J, 2007. Brilliant whiteness in ultrathin beetle scales. Science 315:348-348.

Vukusic P, Sambles JR, 2003. Photonic structures in biology. Nature 424:852-855. doi: 10.1038/nature01941.

Wilts BD, Michielsen K, De Raedt H, Stavenga DG, 2014. Sparkling feather reflections of a bird-of-paradise explained by finite-difference time-domain modeling. Proceedings of the National Academy of Sciences 111:4363-4368. doi: 10.1073/pnas.1323611111.

Xiao M, Dhinojwala A, Shawkey M, 2014. Nanostructural basis of rainbow-like iridescence in common bronzewing *Phaps chalcoptera* feathers. Opt Express 22:14625-14636. doi: 10.1364/OE.22.014625.

Yoshioka S, Kinoshita S, 2002. Effect of macroscopic structure in iridescent color of the peacock feathers. Forma 17:169-181.

Young CM, Cain KE, Svedin N, Backwell PRY, Pryke SR, In Press. The role of pigment based plumage traits in resolving conflicts. J Avian Biol. doi: 10.1111/jav.00742.

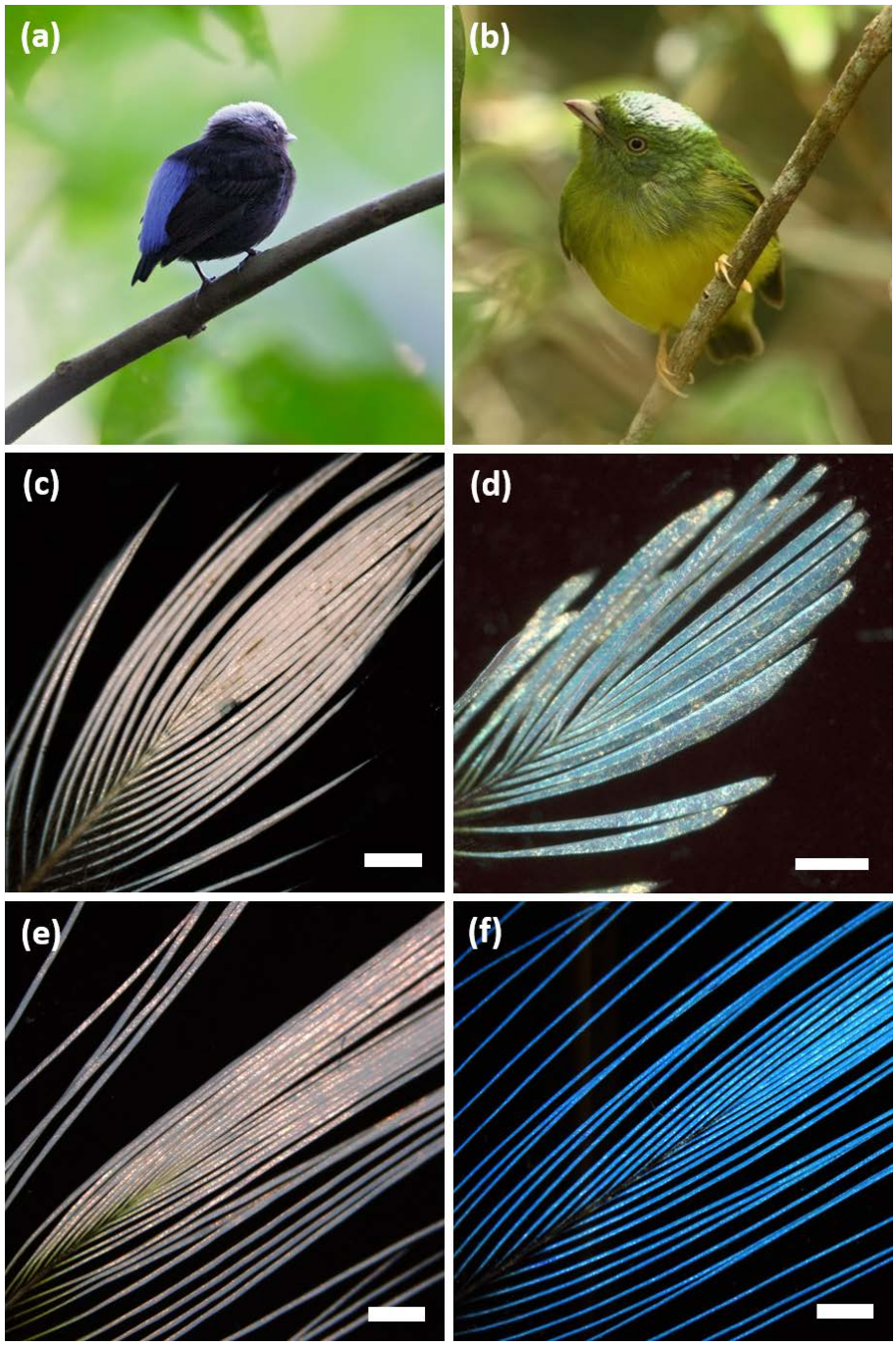

Figure 1. Study species and feathers. Photographs of (a) *L. isidorei* (credit Ben Sadd) and (b) *L. iris* (credit Marcelo Barreiros), as well as (c) *L. isidorei* crown, (d) *L. iris* crown, (e) *L. nattereri* rump, and (f) *L. coeruleocapilla* rump feathers. Scale bars: 0.5 mm.

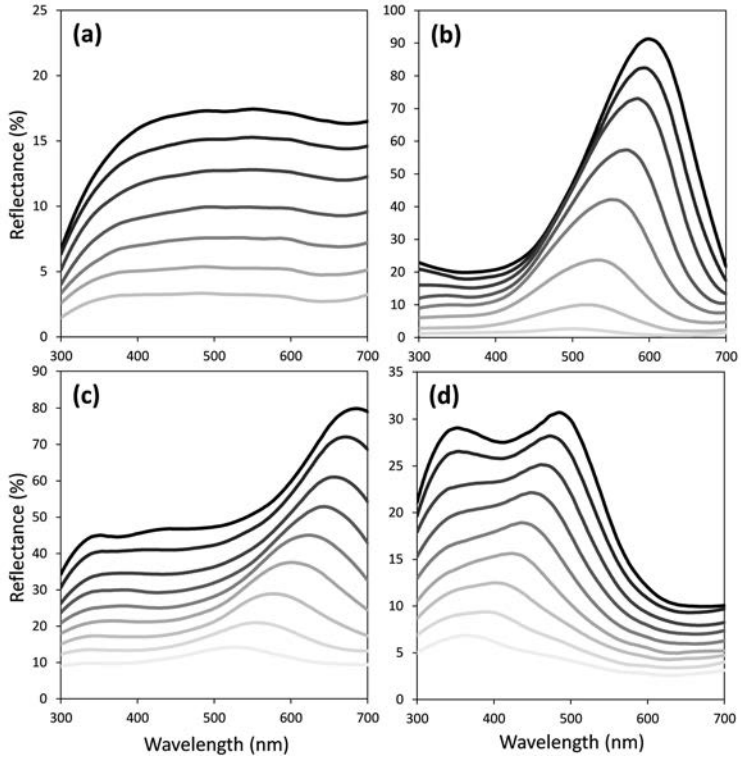

Figure 2 Specular reflectance of individual feathers at 5° angle increments starting at 10° (dark grey), and up to 50° (light gray), from coincident normal (0°): (a) *L. isidorei* crown, (b) *L. iris* crown, (c) *L. nattereri* rump, and (d) *L. coeruleocapilla* rump feathers. Due to small size, crown feathers could only be measured up to 45° from coincident normal.

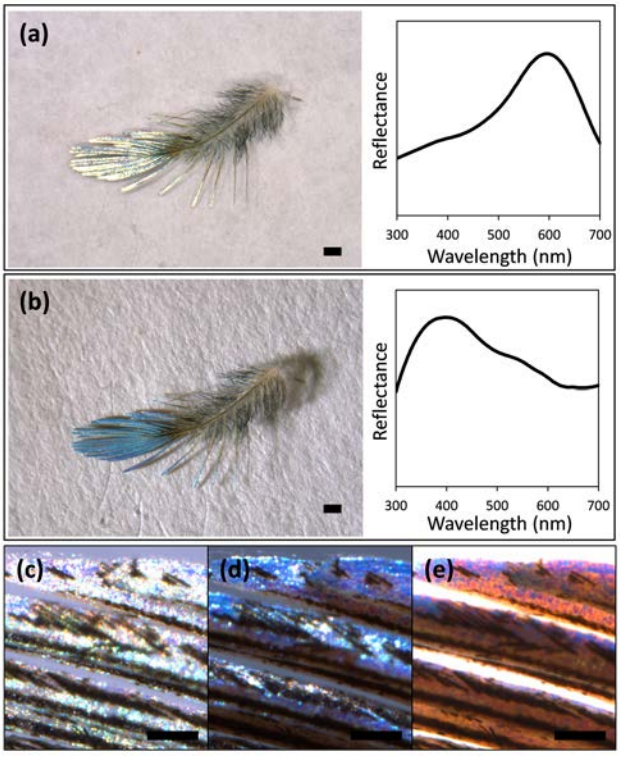

Figure 3. *L. iris* crown feathers at incident light at different viewing geometries: (a & c) normal incidence; (b & d) 45° + 30° from normal incidence; (e) in transmittance. Images show feathers either dorsal side up (a & b) or ventral side up (c-d). Black regions seen in (c-d) are melanised barbules and narrow melanised region of the barb cortex. Scale bars are 0.5 mm (a & b) and 0.1 mm (c-d).

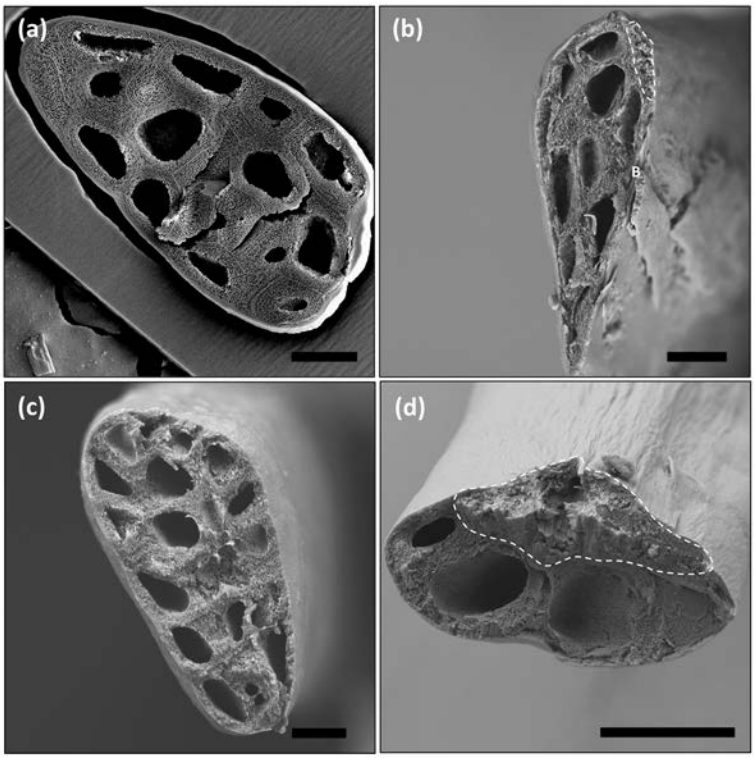

Figure 4. SEM images of whole barb cross-sections for (a) *L. isidorei* crown, (b) *L. iris* crown, (c) *L. nattereri* rump, and (d) *L. coeruleocapilla* rump feathers. Melanised regions of barbs are indicated by dashed lines and the melanised barbule with "B". Scale bars: 10 µm.

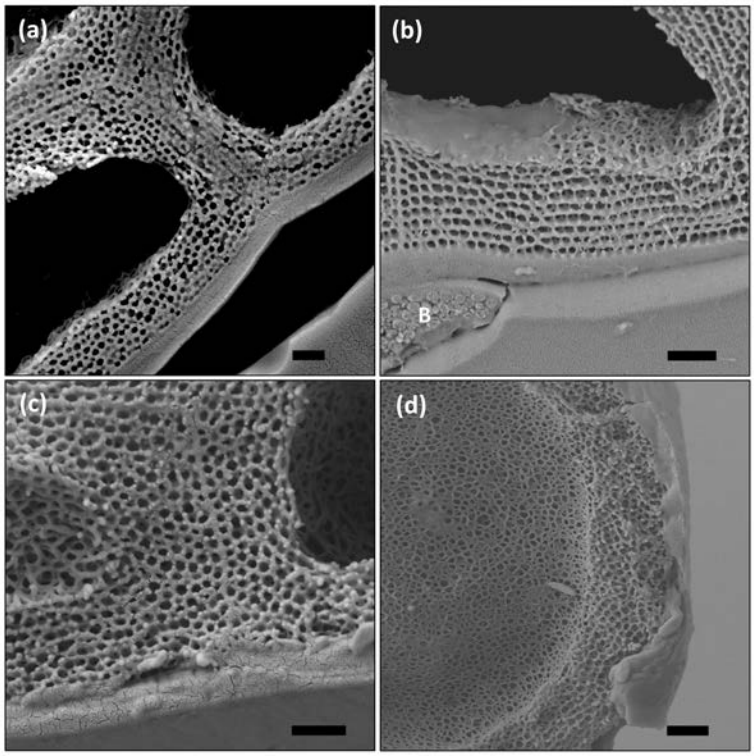

Figure 5. SEM images of barb cross-sections at the junction of the cortex and medulla for (a) *L. isidorei* crown, (b) *L. iris* crown, (c) *L. nattereri* rump, and (d) *L. coeruleocapilla* rump feathers. Melanised barbule is indicated with "B". Scale bars: 1 μm.

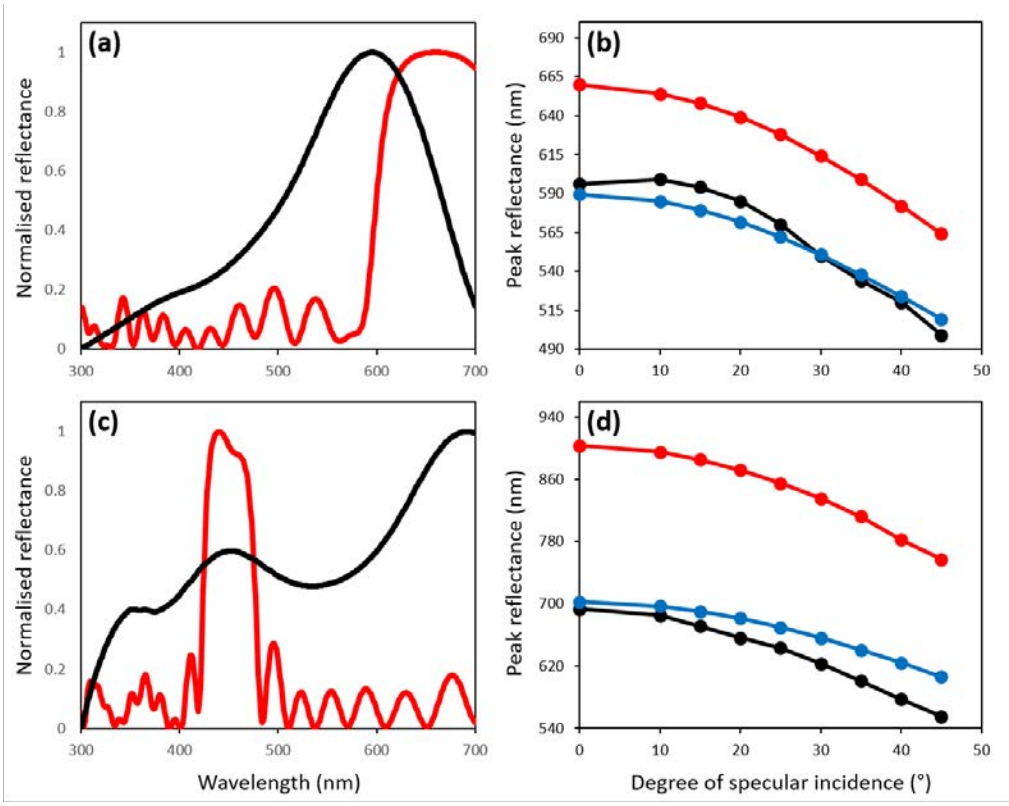

Figure 6. Measured (black lines) and predicted spectral properties predicted using optical models for 3D inverse-opal photonic crystals (blue lines) or 1D multilayers (red lines) for *L. iris* crown (a & b) and *L. nattereri* rump (c & d) feathers at normal incidence (a & c) or across different specular angles (b & d). Note that (c) illustrates the predicted secondary reflectance peak for a 1D multilayer, whereas values in (d) are peak reflectance for the primary peak.

2) **A nanostructural basis for glossy red plumage colors**

Jean-Pierre Iskandar[1*], Chad Eliason[1,2], Tim Astrop[1,3], Branislav Igic[1], Rafael Maia[1,4] & Matthew D. Shawkey[1*]
[1]Integrated Bioscience Department, The University of Akron, Akron, OH USA
[2]Departments of Integrative Biology and Geological Sciences, University of Texas at Austin, Austin, TX USA
[3]Department of Biology & Biochemistry, University of Bath, Bath, BA2 7AY, United Kingdom
[4]Department of Ecology, Evolution and Environmental Biology, Columbia University, New York, NY USA
[*]Author for correspondence: shawkey@uakron.edu
Running title: Morphology of glossy reds

ABSTRACT

Gloss is a common property of materials that usually arises through specular reflection from smooth, flat surfaces. In birds, as in other organisms, colors are produced by pigments, nanostructures that scatter light, or both. Atypically, however, the gloss on black feathers is produced in part by the organization of melanin-containing organelles (melanosomes) under a thin keratin cortex. Brightly colored feathers, including brilliant reds produced by carotenoids, are sometimes comparably shiny. How pigments and feather structure interact to produce gloss on these feathers has never been examined. Here, we compared the optical and structural properties of carotenoid-based red feathers to identify the proximate basis for their glossiness. Glossy red feathers had thicker barbs with a flatter and more homogeneous planar morphology, consistent with expectations, as well as thicker outer keratin cortices. Our results demonstrate that gloss of carotenoid-based red feathers is produced at least in part by barb microstructure and nanostructure, illustrating a novel color-producing interaction that neither pigment nor microstructure could alone attain. Whether and how the ecology and evolution of these colors differs from typical red feathers will be rich areas for future study.

INTRODUCTION

Bright avian plumage colors are some of the most conspicuous signals found in animals, playing important roles in intra- and interspecific communication, as well as camouflage and heat regulation (Hill & McGraw, 2006). Understanding the mechanisms underlying production and maintenance of feather colors is critical to understanding their function (Prum, 2006; Shawkey, Morehouse & Vukusic, 2009; Wilts *et al.*, 2014), the constraints on their production (Shawkey *et al.*, 2015; McGraw, 2006; Galvan & Alonso-Alvarez, 2008), and their evolution (Stoddard & Prum, 2011, Maia, Rubenstein & Shawkey, 2013; Eliason, Maia & Shawkey, 2015). Traditionally, feather colors have been classified as either pigment-based (produced by selective absorption of certain wavelengths of light by molecules, mainly melanins and carotenoids) or structural (produced by differential scattering and interference as light interacts with materials of varying refractive indices; Prum, 2006). However, structural and pigmentary components of coloration often interact to produce colors. For example, in budgerigar (*Melopsittacus undulatus*, Gould, 1840) feathers a pigment selectively absorbs blue wavelengths, enhancing the green color produced by the nanostructured spongy matrix of keratin and air (D'Alba, Kieffer & Shawkey, 2012). In fact, variation in colors traditionally interpreted as "pigment-based" can often be structurally derived (Shawkey & Hill, 2005; Evans & Sheldon, 2012, Jacot *et al.*, 2010, San-Jose *et al.*, 2013), and this variation might be as relevant in signaling and interactions as that controlled by pigment deposition itself.

Most studies of coloration have focused on examining brightness, hue and saturation, while overlooking other properties such as iridescence and glossiness. Gloss, the quality of mirror-like or specular reflectance characteristic of surfaces, is a common component of avian feathers and is usually produced by smooth polished surfaces (Toomey *et al.*, 2010). A few recent studies have brought attention to gloss by attempting to quantify it (Toomey *et al.*, 2010) and identify the morphological features underlying its production (Maia, D'Alba & Shawkey, 2011; Igic *et al*., 2015). Gloss is noticeable on darkly colored surfaces, such as melanin-based black feathers, where specular highlights contrast markedly with the dark diffusely reflected color. However, gloss can also be observed in feathers colored by other pigment types like carotenoids.

From the velvety bib of the House Finch (*Haemorhous mexicanus,* Müller, 1776) to the fiery crests of woodpeckers (Piciformes), carotenoid-based red feathers can vary dramatically in their amount of gloss (Fig. 1). However, the proximate mechanism underlying gloss in red feathers may be dramatically different than that observed in black feathers. This is because the latter is controlled by the degree of organization and continuity in the layer formed by the rod-shaped melanin-containing organelles (melanosomes), as well as by the thickness of the keratin layer that overlays it (Maia *et al.* 2011). Carotenoids and other red pigments, however, are not found in organelles, and instead are diffusely mixed within the keratin matrix of the feather (Shawkey & Hill, 2005; Shawkey *et al.* 2009). Thus, gloss is likely produced by different mechanisms in carotenoid-pigmented feathers.

The objective of this study was to characterize gloss in red-pigmented feathers, and identify the underlying mechanisms responsible for its production and variation. We quantified gloss using angle-resolved spectrometry and compared it between carotenoid-based red feathers visually classified as either glossy or matte. We then identified the morphological basis of gloss by relating it to the morphology and nanostructure of these feathers. Because red carotenoid-based feathers lack discrete organelles to contain pigments, we hypothesized that barb morphology, rather than sub-surface barb or barbule nanostructure would explain glossiness.

METHODS

Sample Collection

Samples of red bird feathers were collected from the ornithological collection of The University of Akron and the Cleveland Museum of Natural History. Twenty-six samples from several avian families were collected and visually classified by four different observers as either matte (n=13) or glossy (n=13). Seven feathers of each bird were collected (see table 1): five were used for spectrometry measurement, and the rest were embedded for light microscopy and transmission electron microscopy (see methods below).

Color measurements

We stacked and taped five feathers directly on top of one another to a holder with a matte black velvet background and measured their reflectance between 300-700 nm (i.e. the bird-visible spectrum) using an Avantes AvaSpec-2048 spectrometer and AvaLight-XE pulsed xenon light source and Avantes WS-2 white standard as a reference. We measured feathers in stacks rather than on study skins to minimize variation due to e.g. curvature of the bird's body. Gloss can be affected by both specular and diffuse reflectance, so we measured both on the same samples using standard techniques. To quantify specular reflectance, we took point-source reflectance measurements using two separate probes both placed at 60°from the plane normal using a block holder (AFH-15, Avantes Inc.). Measuring at this angle minimizes scattering from the bulk material (i.e. pigments, keratin fibers) (Maia et al. 2011, Hunter

1937) and thus maximizes our estimates of gloss. We measured reflectance with the light source oriented parallel to the barbs. A subsample measured with the light source orthogonal to the barbs showed higher reflectance for both glossy and matte feathers (Fig. 2), indicating that sample orientation would similarly affect both sets of samples and therefore likely would not affect our conclusions. We quantified diffuse reflectance with an integrating sphere (AvaSphere-50-REFL, Avantes Inc.) equipped with a black gloss trap to exclude specular reflectance (AvaSphere-GT50, Avantes Inc.). We took three measurements for each species, moving the probe holder slightly between measurements, and averaged the spectra to account for variation in reflectance along the feather surface. We calculated contrast gloss as the ratio of summed specular to summed diffuse reflectance (Hunter's contrast gloss: Hunter, 1937; Maia, 2011; Igic *et al.* 2015). All spectral analyses were done in R using the pavo package (Maia *et al.*, 2013).

Feather microstructure analysis

We examined feathers using light microscopy (LM) and transmission electron microscopy (TEM) to identify the mechanisms for gloss production by red feathers. We embedded the feathers using a standard protocol (described in Shawkey *et al.*, 2003), trimmed blocks with a Leica S6 EM-Trim 2 (Leica Microsystems GmbH, Wetzlar, Germany) and cut 80 nm thick ultrathin sections with an Ultra 45 diamond knife (Diatome Ltd, Biel, Switzerland) on a Leica UC-6 ultramicrotome (Leica Microsystems GmbH, Wetzlar, Germany). We prepared 100-nm thick samples for TEM analysis and 500-nm thick sections for LM. To clearly observe interior structure and pigment distribution, we stained cross-sections with either toluene for LM or ethidium bromide for TEM. We viewed the cross-sections using a Leica light microscope and a JEOL JEM-1230 TEM at an operating voltage of 120 kV. We used ImageJ (http://fiji.sc/Fiji) to measure barb thickness (area in μm^2 occupied by a cross-section); barb curvature at the exposed (visible) portion of the barb surface where we observed maximal gloss (arc length divided by the radius of a circle fit to a set of points along the edge of a barb profile; Berresford & Rockett, 2013); the aspect ratio of barbs (length divided by width, measured at the outermost points of a barb profile); average distance between barbs (measured as the spacing along the rachis between ten consecutive barbs); barb density (measured as the number of barbs divided by the rachis length)the length of the barb ramus covered by barbules (as a proportion of total ramus length). In addition to surface structure, the amount of light reflected from a material may also depend on the thickness of the outermost layer, which could act as a thin-film reflector (Prum 2006). Therefore, in addition to quantifying barb microstructure, we determined the average thickness and coefficient of variation for the thickness of the keratin cortex (Maia *et al.* 2011) at the outer edge of barbs from TEM images.

Geometric morphometrics of barb shape

Digitized images of the barb thin sections where used to investigate variation in cross-sectional shape between the sampled species. Due to the sub-circular outline of the sectioned barbs and lack of multiple, clear anatomically homologous features, traditional landmark based morphometric techniques (Bookstein, 1982) would be inappropriate for these samples. The analysis of outlines via eigenshape shape analysis (sensu MacLeod, 1999) has been successfully implemented in many recent studies (Ubukata *et al.*, 2009; Astrop, 2011; Astrop *et al.*, 2012; Wilson *et al.*, 2013*a*, *b*) to assess morphological variation within and between taxa where such homologous features are absent.

Eigenshape analyses operate via the conversion of the digitized outline of an individual specimen into equidistant, Cartesian (x-y) coordinates. These digitized coordinates are then transformed (removing size, scale and rotation from the analysis) into a shape function as

angular deviations (phi function: φ; Zahn & Roskies, 1972) that describe the shape of the curve. This description is derived from a set of empirical, orthogonal shape functions via an eigenfunction analysis of a matrix of correlations between shapes. Eigenshape scores can then be used to project individual specimens into a multi-dimensional morphospace that allows the interpretation of individual vectors of shape change.

Outlines of the samples were digitized into 20 equidistant points from the apex of curvature at the dorsum of the barb (type II landmark) using tpsDig2 (Rohlf, 2001). Eigenshape analyses were performed using FORTRAN routines written by Norman MacLeod (NHM London). The eigenshape functions in the freely available PAST program (Harper & Ryan, 2001) were implemented for shape visualization.

Statistical analyses

We used statistical models to test whether feather morphology affects observer classifications of glossiness and spectrometric measurements. First, we tested whether human classified glossy and matte feather differed in respect to contrast gloss, diffusely reflected brightness, and specularly reflected brightness. Secondly, we tested whether human classified glossy and matte feather differed in respect to barb thickness, barb curvature, barb cortex thickness, bar density, barbule coverage, and aspect ratio of barbs. To avoid problems of collinearity between morphological measurements, we used principal component (PC) analysis on the correlations matrix of these morphological measurements to reduce them to several orthogonal axes that explain the greatest amount of total variance (Table S1). Prior to PC analysis, we log transformed barb thickness and curvature, and arcsine transformed barbule coverage, to improve their normality. In our analyses, we included the first four PC axes that collectively explained 90% of the total variance. For example, the first PC axis compared the barb thickness, cortex thickness, and density to barb curvature, barb aspect ratio, and barbule coverage, whereas the second PC compared the barb thickness, curvature, and cortex thickness to barb aspect ratio (Table S1). We used penalized maximum likelihood logistic regression to test whether morphological variation explained by the first four PC axes influences the probability that human vision classifies a feather as glossy versus matte (Table S2). Thirdly, we used linear models to test whether morphological variation explained by the first four PC axes influences contrast gloss, diffusely reflected brightness, and specularly reflected brightness (Table S2). We log transformed contrast gloss, diffuse brightness, and specular brightness to improve the normality and homogeneity of variance among residuals.

As shared common ancestry between species can influence the outcomes of comparative analyses, we repeated the above analyses while also controlling for phylogenetic relatedness among species. However, including phylogenetic controls did not affect our results (Tables S3 and S4), and we therefore report results from non-phylogenetically controlled models below.

Finally, we used permutational MANOVAs based on distance metrics to test for differences across eigenshape axes between human classified matte and glossy feathers.

All statistical analyses were conducted in R v3.2.2. We fit linear models using the lm() function in the base package of R and the penalized maximum likelihood logistic regression model using logistf() of the logistf package (Ploner et al. 2013). We conducted phylogenetic PC analysis using the phyl.pca() function of the phytools package (Revell 2012) and phylogenetically controlled general linear models using the phylolm() and phyloglm() of the phylolm package (Ho & Ane 2014). We conducted permutational MANOVAs using the adonis() function and assessed homogeneity of variance among glossy and matte feathers by comparing distances from points to group centroids using the betadisper() function in the vegan package (Oskanen *et al.*, 2015).

RESULTS

Reflectance and Gloss

Our visual classification of feathers as "matte" or "glossy" reflected quantifiable differences in their reflectance properties (Figure 3A). Human-classified matte feathers had diffuse reflectance over twice as high as glossy feathers (estimate ± s.e: -0.78 ± 0.13, t_{23} = -6.06, P < 0.001; Figure 3B), but the two groups did not differ in their specular reflectance (estimate ± s.e: 0.10 ± 0.17, t_{23} = 0.60, P = 0.56; Figure 3C). As a consequence, their contrast gloss significantly differed by a similar magnitude to that of diffuse reflectance measurements (estimate ± s.e: 0.88 ± 0.14, t_{23} = 6.23, P < 0.001; Figure 3D).

Gloss and Feather Morphology

The morphology of human classified matte and glossy red feathers differed. Glossy feathers had barbs that were flatter, thicker, less covered by barbules, and had thicker cortices (PC1: estimate ± s.e: 1.75 ± 0.78, $\chi_1^2 = 16.65$, P < 0.0001; Table 2, S2).

Feather morphology also affected the reflectance properties of red feathers. Diffuse reflectance decreased (PC1: estimate ± s.e: -0.23 ± 0.04, t_{20} = -5.28, P <0.0001; Figure 4A; Table S2) , while contrast gloss increased (PC1: estimate ± s.e: 0.26 ± 0.05, t_{20} = 5.04, P <0.0001; Figure 4D; Table S2) as barbs were flatter, thicker, with thicker cortices, and were less covered by barbules. In addition, diffuse reflectance decreased as barbs were rounder with lower aspect ratios (PC2: estimate ± s.e: -0.13 ± 0.06, t_{20} = -2.41, P = 0.03; Figure 4B; Table S2). By contrast, specular reflectance was not associated with any morphological measurements (all P > 0.05; Figure 4C; Table S2).

Gloss and Barb Geometric Morphometrics

Matte and glossy barbs differed significantly in their overall shape based on the first three axes of shape variation (permutational MANOVA: $F_{1, 23}$ = 4.26, P = 0.005, R^2 = 15.65%; Figure 5) and did not differ in levels of within-group variation (analysis of multivariate homogeneity of group dispersions: $F_{1, 23}$ = 1.79, P = 0.19). The first three eigenshapes account for 64% of the observed variation within the dataset. Eigenshape 1 highlights changes in shape of the ventral width of the barb and accounts for 30% of the shape variation. Eigenshape 2 (accounting for 22% of the shape variation) described changes in the width toward the dorsal apex of the barb. Eigenshape 3 described changes in the overall width, centred toward the middle of the barb, accounts for 12% of the captured variation in shape and. The third eigenshape (describing differences on the curvature of the midsection of the barb cross-section, Figure 5) was the only significant predictor of contrast gloss such that glossy feathers had flatter (less concave) barb midsections (estimate ± s.e: 0.23 ± 0.11, t_{20} = 2.11, P < 0.05; Figure 5; Table S5).

DISCUSSION

Gloss has been studied extensively in, for example, human hair () and synthetic materials (), but sparsely in eggs (Igic et al. 2015) and feathers (Toomey et al. 2010, Maia et al. 2011). Glossy surfaces in all these cases are typified by high specular reflectance. Thus, we expected glossy red feathers to have higher specular reflectance than matte feathers, but they did not. Instead, they had lower diffuse reflectance, leading to higher gloss as defined as the ratio of specular to diffuse reflectance. Our morphological analyses of glossy and matte feathers revealed distinct differences in barb shape that were strongly associated with matte and glossy feather types. Form-function analyses of these morphotypes showed that large, flat barbs reflect light more strongly in the specular direction, whereas smaller, curved barbs reflect light diffusely in multiple directions. One possible reason for the positive relationship

between barb size and glossiness is that large barbs result in greater surface area for light reflection (Marschner, 2004; Keis et al. 2004); lower barb density would cause diffuse scattering from barb edges. The negative relationship between barb ramus curvature and glossiness is consistent with optical theory, as curved (convex) surfaces scatter light more diffusely than flat surfaces, leading to lower gloss (Hecht & Zajac, 1974; Barkas, 1939). A similar effect has recently been described in dragonfly wings (Nixon, Orr & Vukusic, 2015). The presence of barbules may enable a smooth, continuous sheet-like orientation of barbs via interlocking hooklets and at the same time increase diffuse scattering, which could potentially explain why barbules were positively associated with both specular and diffuse reflectance, but not gloss (Fig. 4).

The positive relationship between gloss and cortex thickness indicates that nanostructure may play a role in gloss production. Interestingly, the buttercup flower (*Ranunculus repens*, Linnaeus, 1753) produces glossy yellow color through specular reflection from a smooth outer surface containing pigments (Vignolini *et al*. 2012). However, red feathers have carotenoids distributed throughout their barbs, so it is unlikely that they share this mechanism with buttercups. Keratin cortices in glossy red feathers are ~65 nm thinner on average than those that contribute to glossy color in black feathers (Maia et al. 2011), but are nevertheless within the proper size range to produce color by thin film interference (Hecht and Zajac, 1974; Shawkey et al. 2009). However, the refractive index contrast between the cortex and the underlying keratin in red feathers, unlike that between the cortex and melanosomes in glossy black feathers, is likely low. Thus, reflectance from this layer should be weak, but more data on refractive indices (e.g. Wilts et al.) are needed to state this more definitively

Variation in carotenoid concentration may also affect glossiness. Because they absorb light (McGraw 2006), higher concentrations of carotenoids should strongly reduce diffuse reflectance. This would lead to a darker background reflectance against which specular reflectance would be more visible. Indeed, this may explain why diffuse reflectance of glossy feathers was lower than, and specular reflectance was unexpectedly similar to, that of matte feathers. Furthermore, it would explain why only reflection at longer wavelengths (~600-700 nm), where carotenoids do not absorb, are strongly angle-dependent (Figure 2): gloss may be most visible in wavelengths where its effects are not diluted by absorbance from carotenoids. Analyzing relative carotenoid content of these feathers will enable us to test this hypothesis in the future.

Taken together, these results imply that barb morphology, barbule presence/absence and carotenoid concentration collectively contribute to produce gloss. However, the precise optics of this system remain to be examined in the future. Furthermore, the unexpectedly high levels of variation in barb ramus shape (exemplified in figs. 1,4) observed in this study raise further questions about the diversity, development and genetic determinants of these relatively unexplored feather barb morphologies. For example, whether other glossy carotenoid-containing (e.g. yellow tail feathers of cedar waxwings *Bombycilla cedrorum*), and/or structurally-colored feathers (e.g. blue feathers of fairy bluebirds *Irena* spp.) feature similar modifications will be interesting to test.

Animal signals are complex, multimodal phenotypes characterized by their color, form, and motion (Grether, Kolluru & Nersissian, 2004). Carotenoid-based colors in birds are diverse (Stoddard & Prum, 2011) and thought to have evolved by sexual selection for their signaling functions (Hill, 2006). In addition to the considerable variation in the form and color of carotenoid-based plumage traits (Stoddard & Prum, 2011), our results suggest that the dynamic character of glossiness is similarly variable and broadly distributed throughout Aves (see Table 1). Our mechanistic work shows that glossiness of red feathers is produced by numerous aspects of feather morphology, and can therefore vary independently of chromatic

color attributes (e.g. hue), potentially allowing birds to convey unique information to receivers about their quality or motivation to mate. Testing if and how these different attributes (color and glossiness) act as redundant signals or interact to determine mating success remains to be explored (see Hebets & Papaj, 2005). Glossiness is a highly directional trait (changing with viewing angle), and birds may be able to flash these signals on and off similar to iridescent traits (Osorio & Ham, 2002; Meadows *et al*., 2011). Interestingly, many glossy feathers are found on crests (Table 1), which can sometimes be dynamically raised and lowered, potentiating iridescent signaling. Recent work suggests that directional signals cause a strong link between the environment (e.g., lighting conditions) and signaling behavior (Dakin & Montgomerie, 2009; Siscu *et al.*, 2013) that might drive the evolution of display behavior. Glossiness may therefore play an important, but largely overlooked, role in sexual selection of carotenoid-based bird colors (e.g., Toomey *et al.,* 2010; Maia *et al.*, 2011). These results increase our understanding of the structural mechanisms behind glossiness and provide a framework for future studies on the ecology and evolution of glossy, carotenoid-colored feathers.

REFERENCES

Andersson S. **1999**. Morphology of UV reflectance in a whistling-thrush:implications for the study of structural colour signalling in birds. *Journal of Avian Biology* **30:** 193–204.

Astrop TI. 2011. Phylogeny and Evolution of Mecochiridae (Decapoda: Reptantia: Glypheoidea): An Integrated Morphometric and Cladistic Approach. *Journal of Crustacean Biology* **31**: 114–125.

Astrop T, Park L, Brown B & Weeks SC. **2012.** Sexual discrimination at work: Spinicaudatan'Clam Shrimp'(Crustacea: Branchiopoda) as a model organism for the study of sexual system evolution. *Palaeontologia Electronica* **15**: 2.20A.

Auber L. 1957. The structures producing "non-iridescent" blue color in bird-feathers. *Proceedings of the Zoological Society of London* **129:** 455-486.

Barkas WW. **1939**. Analysis of light scattered from a surface of low gloss into its specular and diffuse components. *Proceedings of the Physical Society* **51:** 274.

Berresford GC & Rockett AM (eds.). 2013. *Applied calculus: sixth edition*. Boston, MA: Brooks/Cole.

Bookstein F. 1982. Foundations of morphometrics. *Annual Review of Ecology and Systematics* **13**: 451-70.

Chandler A. 1916. A study of the structure of feathers: With reference to their taxonomic significance. *University of California Publications in Zoology* **13:** 243–447.

D'Alba L, Kieffer L & Shawkey MD. 2012. Relative contributions of pigments and biophotonic nanostructures to natural color production: a case study in budgerigar (*Melopsittacus undulatus*) feathers. *The Journal of Experimental biology* **215**: 1272-1277.

Dakin R & Montgomerie R. 2009. Peacocks orient their courtship displays towards the sun. *Behavioral Ecology and Sociobiology*. **63**: 825-834.

Eliason CM, Maia R & Shawkey MD. 2015. Modular color evolution in birds facilitated by a complex nanostructure. *Evolution* **69**: 357-367.

Evans SR & Sheldon BC. 2012. Quantitative genetics of a carotenoid-based color: Heritability and persistent natal effects in the Great Tit. *American Naturalist* **179**:79-94

Frank VF. 1939. Die Färbung der Vogelfeder durch Pigment und Struktur. *Journal of Ornithology* **87:** 426–523.

Galván, I & Alonso-Alvarez C. 2008. An intracellular antioxidant determines the expression of a melanin-based signal in a bird. Public Library of Science One **3**: e3335

Grether GF, Kolluru GR & Nersissian K. 2004. Individual colour patches as multicomponent signals. *Biological Reviews* **79**: 583–610.

Harper D & Ryan P. 2001. PAST: paleontological statistics software package for education and data analysis. *Palaeontologia Electronica* **4**: 1–9.

Hebets EA & Papaj DR. **2005**. Complex signal function: developing a framework of testable hypotheses. *Behavioral Ecology and Sociobiology* **57**: 197–214.

Hecht E & Zajac A. 1974 *Optics*. New York, NY: Addison- Wesley.

Hill GE. 2006. Female mate choice for ornamental coloration. In McGraw KJ & Hill GE, eds. *Bird Coloration: Volume II*. Cambridge, MA: Harvard University Press, 137–200.

Hill GE & McGraw KJ, eds. 2006 *Bird Coloration, Vol. 1 :Mechanisms and Measurement*. Cambridge, MA: Harvard University Press.

Hunter R.S., **1937.** Methods of determining gloss. *Journal of Research of the National Bureau of Standards* **18**: 19-39.

Igic B, Fecheyr-Lippens DC, Chan A, Hanley D, Brennan P, Grim T, Waterhouse GIN, Hauber ME, Shawkey MD. 2015. A nanostructural basis for gloss of avian eggshells. *Journal of The Royal Society Interface* **12**: 1210-1215.

Jacot A, Romero-Diaz C, Tschirren B, Richner H & Fitze PS. 2010. Dissecting Carotenoid from Structural Components of Carotenoid-Based Coloration: A Field Experiment with Great Tits (Parus major). *American Naturalist* **176**: 55-62

Keis K, Ramaprasad K & Kamath Y. 2004. Studies of light scattering from ethnic hair fibers. *Journal of Cosmetic Science* **55**: 49–63.

Macleod N. 1999. Generalizing and Extending the Eigenshape Method of Shape Space Visualization and Analysis. *Paleobiology* **25**: 107–138.

Maia R, D'Alba L & Shawkey MD. 2011. What makes a feather shine? A nanostructural basis for glossy black colours in feathers. *Proceedings of the Royal Society B: Biological Sciences* **278**: 1973-1980.

Maia R, Rubenstein DR & Shawkey MD. 2013a. Key ornamental innovations facilitate diversification in an avian radiation. *Proceedings of the National Academy of Sciences USA* **110**:10687–10692.

Maia R, Eliason CM, Bitton PP, Doucet SM & Shawkey MD 2013b. Pavo: an R Package for the Analysis, Visualization and Organization of Spectral Data. *Methods in Ecology and Evolution* **4:** 906-913.

Marschner SR, Jensen HW, Cammarano M, Worley S. & Hanrahan P. 2003. Light scattering from human hair fibers. *ACM Transactions on Graphics (TOG)* **22:** 780–791.

McGraw KJ. 2006. Mechanics of melanin-based coloration. In McGraw KJ & Hill GE, eds. *Bird Coloration: Volume II*. Cambridge, MA: Harvard Univ. Press, Cambridge: Harvard University Press, 243-294.

Meadows MG, Morehouse NI, Rutowski RL, Douglas JM & McGraw KJ. 2011 Quantifying iridescent coloration in animals: a method for improving repeatability. *Behavioral Ecology and Sociobiology* **65**:1317–1327.

Nixon MR, Orr AG & Vukusic P. 2014. Wrinkles enhance the diffuse reflection from the dragonfly *Rhyothemis resplendens*. *Journal of the Royal Society Interface* **12:** 749-755.

Oksanen J, Guillaume Blanchet F, Kindt R, Legendre P, Minchin PR, O'Hara RB, Simpson GL, Solymos P, Henry M., Stevens H. & Wagner H. 2015. vegan: Community Ecology Package. R package version 2.3-1. http://CRAN.R-project.org/package=vegan

Osorio D, Ham A. 2002. Spectral reflectance and directional properties of structural coloration in bird plumage. *Journal of Experimental Biology* **205**: 2017-2027.

Prum RO. 2006. Anatomy, physics and evolution of avian structural colors. In McGraw KJ & Hill GE, eds. *Bird Coloration: Volume II*. Cambridge, MA: Harvard Univ. Press, Cambridge: Harvard University Press.

Rohlf JF. 2001. TPSDig2: A Program for Landmark Development and Analysis.

San-Jose LM, Granado-Lorencio F, Sinervo B & Fitze PS. 2013. Iridiphores and not carotenoids account for chromatic variation of carotenoid-based coloration in common lizards. *American Naturalist* **181**: 396-409

Shawkey MD, Estes AM, Siefferman LM & Hill GE. 2003. Nanostructure predicts intraspecific variation in ultraviolet-blue plumage colour. *Proceedings of the Royal Society B* **270**: 1455-1460.

Shawkey MD, Morehouse NI & Vukusic P. 2009. A protean palette: colour materials and mixing in birds and butterflies. *Journal of the Royal Society Interface* **6:** S221–S231.

Shawkey MD & Hill GE 2005. Carotenoids need structural colours to shine. *Biology Letters* **1** :121-124.

Shawkey MD, D'Alba L, Xiao M, Schutte M & Buchholz, R. 2014. Ontogeny of an Iridescent Nanostructure Composed of Hollow Melanosomes. *Journal of Morphology* **276**: 378-384.

Stavenga DG, Stowe S, Siebke K, Zeil J. & Arikawa K. 2004. Butterfly wing colours: scale beads make white pierid wings brighter. *Proceedings of the Royal Society B* **271**: 1577–1584.

Siscu P, Manica LT, Maia R & Macedo RH. 2013. Here comes the sun: multimodal displays are associated with sunlight incidence. *Behavioral Ecology and Sociobiology* **67**: 1633-1642.

Stettenheim PR. **2000.** The integumentary morphology of modern birds—an overview. *American Zoologist* **40**: 461–477.

Stoddard MC & Prum RO. 2011. How colorful are birds? Evolution of the avian plumage color gamut. *Behavioral Ecology* **22**: 1042–1052

Toomey, M.B., Butler, M.W., Meadows, M.G., Taylor, L.A., Fokidis, H.B., McGraw, K.J., 2010. A novel method for quantifying the glossiness of animals. *Behavioral ecology and Sociobiology* **64**: 1047-1055.

Ubukata T, Tanabe K, Shigeta Y, Maeda H. & MAPES RH. 2009. Eigenshape analysis of ammonoid sutures. *Lethaia* **43**: 266–277.

Vignolini S, Thomas MM, Kolle M, Wenzel T, Rowland A, Rudall PJ, Baumberg JJ, Glover BJ & Steiner U. 2012 Directional scattering from the glossy flower of Ranunculus: how the buttercup lights up your chin. *Journal of The Royal Society Interface* **9**: 1295-1301.

Wilson L, Furrer, H, Stockar R & Sanchez-Villagra M. 2013*a*. A quantitative evaluation of evolutionary patterns in opercle bone shape in Saurichthys (Actinopterygii: Saurichthyidae). *Palaeontology* **56**: 901–915.

Wilson L, Colombo M, Reinhold, H, Salzburger, W. & Sanchez-Villagra, M. 2013*b*. Ecomorphological disparity in an adaptive radiation: opercular bone shape and stable isotopes in Antarctic icefishes. *Ecology and Evolution* **3**: 3166–3182.

Wilts BD, Michielsen K, De Raedt H & Stavenga DG 2014. Sparkling feather reflections of a bird-of-paradise explained by finite-difference time-domain modeling. *Proceedings of the National Academy of Sciences USA* **111**: 4363-4368.

Zahn C & Roskies R 1972. Fourier Descriptions for Plane Closed Curves. *IEEE Transactions on Computers.* **C21**:269–281.

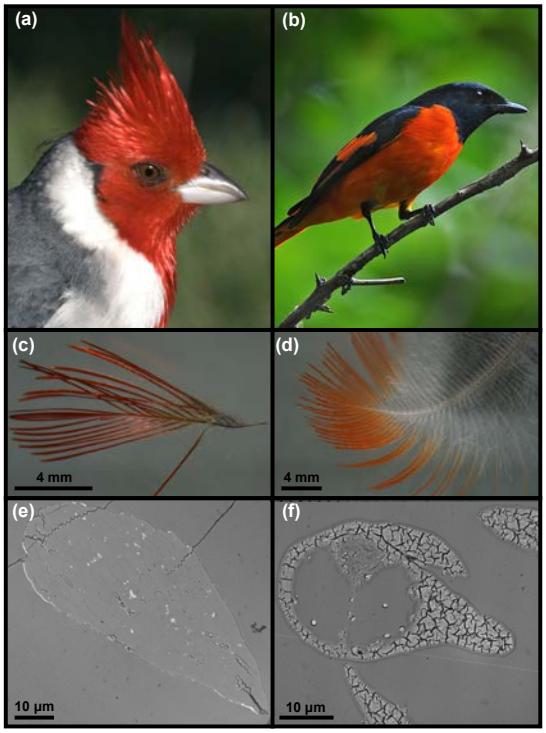

Figure 1. Comparison of representative glossy and matte red feathers. (a)-(b): Pictures of Red-Crested Cardinal (*Paroaria coronata*) and Scarlet Minivet (*Pericrocotus speciosus*). (c)-(d) single feather from the crown of (a) and breast of (b). (e)-(f) TEM image of cross section of barbs (and barbules in (f)) from feathers (c) and (d).

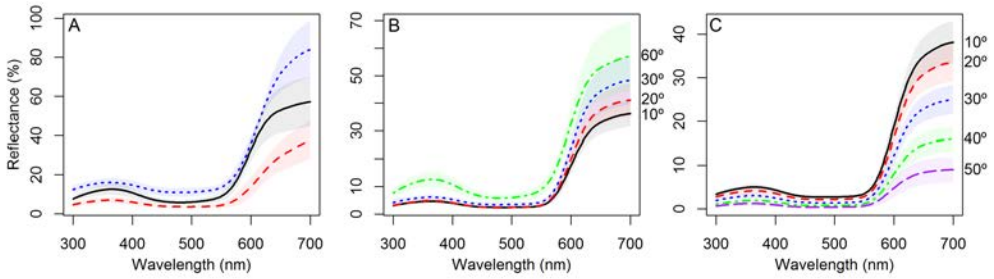

Figure 2. Mean specular reflectance spectra for five representative species measured at three different viewing geometries and orientations relative to the spectrometer setup. (A) Feather orientated such that light and spectrometer probes were positioned either orthogonal to the feather rachis (black line) or parallel to the feather rachis with light being reflected from the feather in a proximal-to-distal direction (red line) or distal-to-proximal direction (blue-line). (B) Reflectance of feathers at different specular angles (10-60º from incident normal). (C) Light scattering spectra for feathers where incident light was maintained at 10º from normal but measurement angle varied between10-50º from normal. Shaded areas illustrate standard errors.

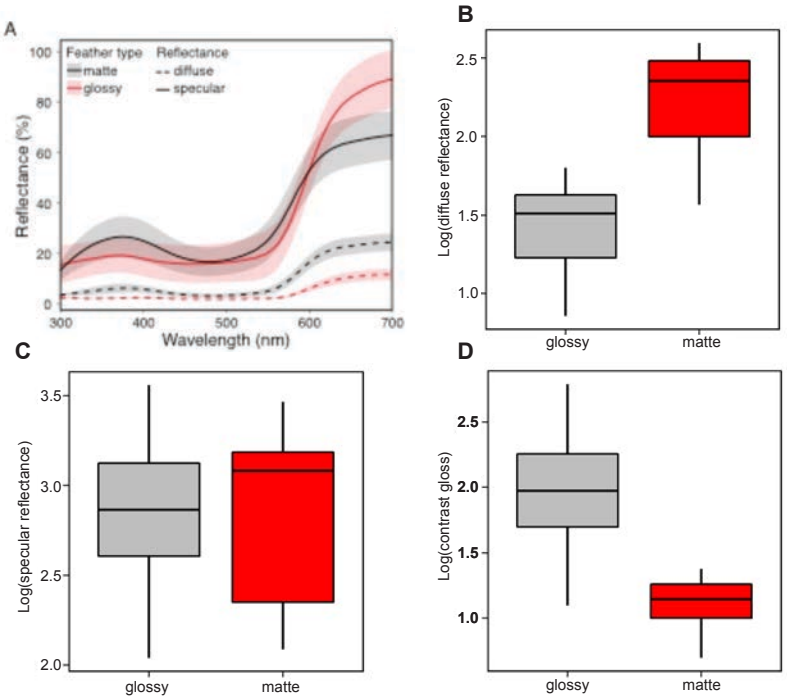

Figure 3. Quantitative assessment of glossiness in red feathers. (a) Mean specular (solid lines) and diffuse reflectance spectra (dashed lines) of glossy (red) and matte feathers (black); shaded bands are ±1 standard error. Boxplots of log diffuse reflectance (b), log specular reflectance (c) and log gloss ratio (specular:diffuse reflectance; d) in glossy and matte feathers.

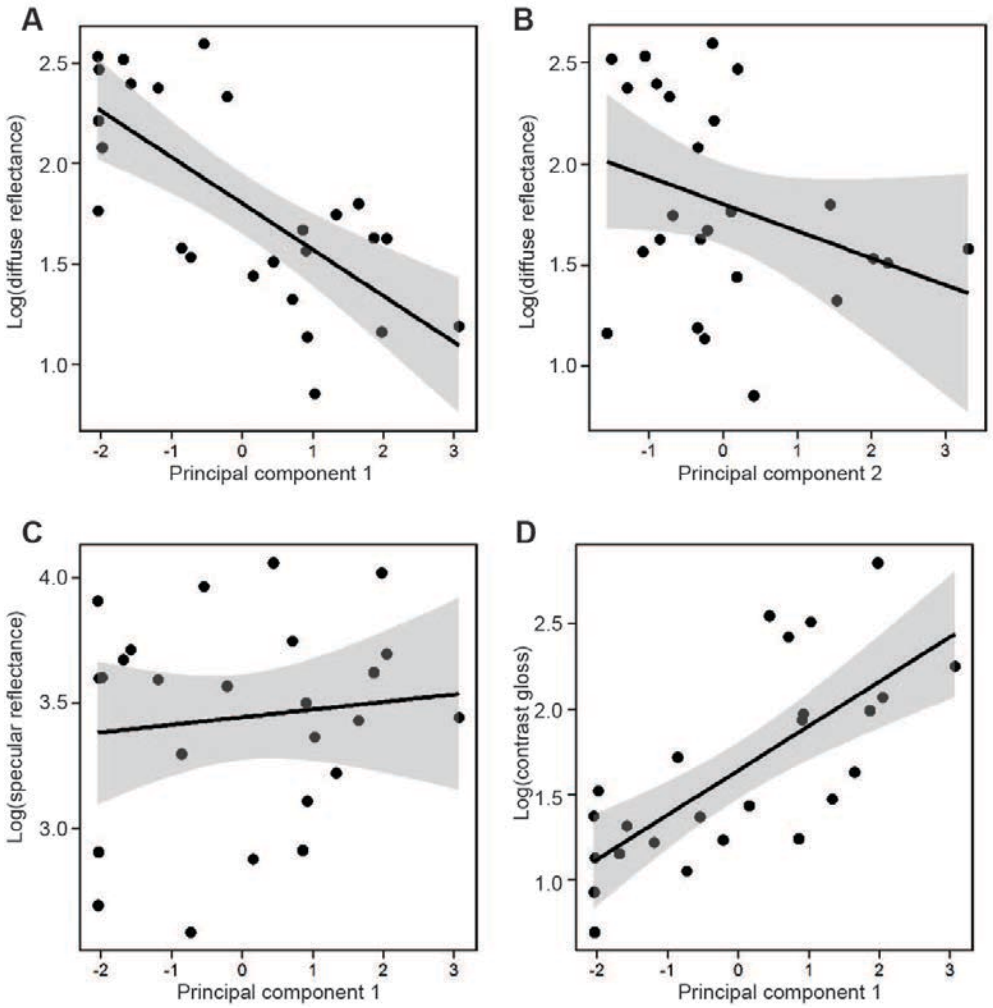

Figure 4. Relationship between morphology and spectral properties of red feather. Conditional plots showing the relationship between log contrast gloss and PC 1 (a), log diffuse brightness and PC 1 (b) or PC 2 (c), and log specular brightness and PC 1 (d). PC 1 compared the barb thickness, cortex thickness, and density to barb curvature, barb aspect ratio, and barbule coverage and accounted for 39 % of total morphological variance, whereas PC 2 compared the barb thickness, curvature, and cortex thickness to barb aspect ratio and accounted for 24 % of total morphological variance (Table S1). Shaded regions are 95% confidence bands.

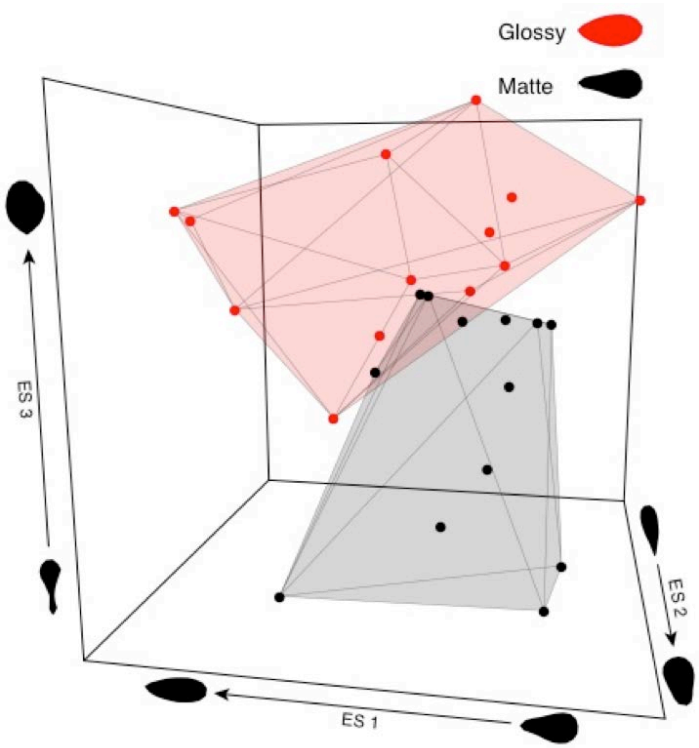

Figure 5. Three dimensional morphospace of barb shape constructed using the first three major axes of variation captured via eigenshape analysis. Polygonal convex hulls illustrate occupied space of both glossy and matte groupings. Sillouettes on axes represent barb shapes at extremes of either eigenshape.

Progress on objective II:

1) Bio-Inspired fast humidity-responsive dynamic structural colors in films of synthetic melanin nanoparticles

Ming Xiao, Yiwen Li, Jiuzhou Zhao, Zhao Wang, Min Gao, Nathan Gianneschi, Ali Dhinojwala, Matthew Shawkey

Department of Polymer Science, The University of Akron, Akron, Ohio 44325, United States
Department of Chemistry & Biochemistry, University of California, San Diego, La Jolla, California 92093, United States
Liquid Crystal Institute, Kent State University, Kent, Ohio 44242, United States
Department of Biology and Integrated Bioscience Program, The University of Akron, Akron, Ohio 44325, United States

Introduction

Colors in nature have functions ranging from warning coloration (aposematism), to interspecific communication and protection from ultraviolet radiation.[1][More ref]_ENREF_1 However, one of the most critical functions of color and color pattern is camouflage from potential predators or prey.[2] Dynamic, changeable colors enable animals to camouflage themselves in variable or numerous environments. One of the best examples, Cuttlefish, changes its skin color, pattern and texture to precisely match its background.[3] Such color changes are facilitated by the use of structural colors arising from nanostructures, as these can be easily tuned by varying the periodic spacing within the nanostructure. Although cuttlefish skin is likely under direct neural control (Ref), extrinsic factors like humidity affect spacing and thus color in other organisms. Structural colors of, for example Morpho butterfly wings,[4] tree swallow feathers,[5] and Hercules beetle elytra[6] change with relative humidity. Similarly, researchers have produced humidity-responsive synthetic optical materials using two strategies, one based on 1D thin-film/multilayer structures and the other based on 3D opal or inverse opal structures. Most 1D photonic crystal structures contain an inorganic/organic hybrid multilayer because the inorganic material, such as titania, offers a higher refractive index than pure organic materials.[7-9] Most humidity induced dynamic colors in opal or inverse opal structures are made with hydrogels that absorb moisture as humidity increases, changing the periodic domain spacing and effective refractive index of the material.[10-12] Replacing hydrogels with natural materials like silk-fibroin only causes as small color change as 20 nm wavelength shift when increasing relative humidity from 30% to 80%.[13] A simpler approach for using a single biocompatible/biodegradable material for dynamic colorimetric performance would be beneficial.

Inspired by the extensive use of melanin particles (sub-micron scale organelles called melanosomes) to create structural colors in birds, we recently demonstrated that synthetic melanin particles offer the same rare combination of high refractive index and high absorption as natural melanin.[14] Here, we show that self-assembled thin films of synthetic melanin particles produce a sensitive color response to changes in humidity. This is because, as we show for the first time, these particles are hygroscopic, absorbing around 13% of water in mass. This absorption changes the thickness of the melanin layer, leading to changes in thin film interference and hence changes in color.

Experiment section

1. SMNP film

Synthetic melanin nanoparticles with diameter of about 200 nm of were synthesized by oxidation and polymerization of dopamine in a mixture of 50 mL water, 20 mL ethanol and 1.2 mL ammonia aqueous solution (30%) at 25℃.[14] The melanin nanoparticles were dispersed in deionized water to make a 1 mg/mL solution. Both transmission electron microscopy (JEM-1230, JEOL Ltd.) and dynamic light scattering measurement (BI-HV Brookhaven instrument with a 633 nm solid-state laser) were used to characterize size and distribution of synthetic melanin nanoparticles.

Silicon wafers (University Wafer) were cleaned using piranha solution (a mixture of H_2SO_4 and H_2O_2 with volume ration of 3:1) at 80°C. A multiple wavelength mode ellipsometer (J.A. Woollam Corp.) was used to measure the thickness of the SiO_2 layer on top of silicon wafer. Clean wafers were held vertically in a SMNP solution at 60°C and SMNP were deposited via capillary flow onto the wafer as the water evaporated. All chemicals were purchased from Sigma-Aldrich. The deposited films were cut in half and both top-view and side-view SEM images were obtained using JEOL-7401scanning electron microscope (JEOL Ltd.) without sputter coating.

2. Humidity response

A CRAIC AX10 UV visible-NIR microspectrophotometer (MSP) (CRAIC Technologies, Inc., a 15 objective, range 400-800 nm) was used to measure the normal reflectance spectra of deposited films in a custom-built humidity chamber (setup in Figure S1). A traceable hydrometer meter with accuracy of 1.5%RH was used to monitor the relative humidity (RH) in the chamber. RH in the chamber was varied from 10% to 90% by controlling the mixing ratio of dry and wet nitrogen gas. Reflectance of films was measured at five humidity points (10%, 30%, 50%, 70%, and 90%) after 1 minute of equilibrium time. For each humidity points, three measurements were performed using a 1 minute interval between each measurement. To investigate how fast the color changes, we recorded the color change (both real-time optical image and spectrum scan) during wetting (10% to 85%) and drying (90% to 10%) process. It took ~50 seconds to reach 85% RH from 10% RH and only 30 seconds to decrease RH below 10% from 90%. We also tested the cyclability of color change by measuring the spectra when wetting and drying the films eight times. To test if the blank silicon reflectance spectrum was influenced by humidity, we measured reflectance of the bare silicon wafer at 10% and 90% RH condition.

3. Water absorption measurement

To quantify how much water SMNP can absorb, we used a CAHN 21 automatic electrobalance (CAHN/Ventron) with an accuracy of ± 0.005% to measure the mass change of small amounts (2~3 mg) of SMNP powder under different humidity conditions. First, we measured the water uptake of three empty standard aluminum DSC pans (13.65 ± 0.02 mg at RH 10%) separately at various RH and we found the changes in mass due to water condensation on the Al pans was small and consistent among individual pans (Figure S5). The net water uptake by the melanin particles can be calculated by subtracting the water uptake by the DSC pan at certain RH. For a specific RH condition, we mixed dry and wet nitrogen gas to reach equilibrium and then started to record the mass every 3 minutes until the variations among the five continuous readings are smaller than 0.010 mg. We repeated the measurements of two separate SMNP samples for both drying and wetting process.

4. Environmental SEM

ESEM (FEI Quanta FEG 450) was used to quantify the thickness change of deposited SMNP films at different humidity change. First, the air pressure in the chamber of ESEM was pumped down to ? Torr and then we increased the pressure to different values by releasing water vapor into the chamber and obtained the images of the same spot. We took measurements at pressure of

Results and Discussion

SMNPs with diameter of 192 ± 10 nm were synthesized and SMNP films producing blue and red structural colors were obtained via evaporative assembly process using the previously described procedure (Figure 1).[14] The size of the homogenous films is at least 0.5 mm × 0.5 mm and cross-sectional SEM shows that the blue film is 274 ± 11 nm and the red film is 602 ± 17 nm thick. Fast Fourier power spectra of the SEM images (top view) show that SMNP formed quasi ordered structures (Figure 1). These films displayed clearly visible dynamic color changes at various RH of 10%, 30%, 50%, 70% and 90% (Figure 2). The color of the blue film shifts to green, with maximum position of the primary peak shifting from 475 nm to 530 nm when RH increased from 10% to 90%. The normal reflectance spectrum of the red film showed two peaks, a major peak at 638 nm and a secondary peak at 483 nm when the RH was 10%. When the RH was increased to 90%, the red film turned green because the major peak shifts to 714 nm and the secondary peak shifts to 551 nm, making the secondary peak more dominant within the human visible wavelength region (400-700 nm[15]). The maximum peak position increased almost linearly as a function of RH (Figure S2). The reflectance spectra for bare wafer under RH of 10% and 90% were virtually identical (Figure S3), demonstrating that the dynamics colors of SMNP films are due to changes in the SMNP layer. The color changes were reversible when the humidity was reduced back to 10%. The video recording the real-time change in color and the shift in the reflectance spectrum is provided in the Supporting Information. The changes in colors were much faster than the changes in humidity (30 seconds during drying from RH 90% to 10% and 50 seconds to increase from RH 10% to 85%). We measured the cyclic response by increasing and decreasing the RH eight times. The position of the maximum peak is reversible (Figure 3 and Figure S4) and we found no change in color saturation or the broadening of the reflectance spectra after eight cycles, which is more advantageous over humidity sensors with broadening peaks under increased RH.[9, 10] Add color analysis in a color space?

Many colorimetric humidity sensors show visible color changes and these results have been attributed to swelling of the 1D or 3D photonic structures. However, no evidence has directly supported this assumption.[7, 9, 11] Here, we were able to monitor the thickness expansion of SMNP film under different humid conditions using environmental SEM (ESEM). We measured the cross-sections of a SMNP film equilibrated at certain water vapor pressure at room temperature (24℃) and calculated the relative humidity by dividing the water pressure by saturated water pressure (22.31 Torr at 24℃). Figure 4 shows the changes in thickness of the melanin film when water pressure is increased from 1 Torr to 5 Torr and then to 10 Torr (RH 4.5%, 22.4% and 44.8%). As a control we measured the changes in the thickness of the SMNP film after exposing the film to a dry N_2 environment. There were no visible changes in the thickness using dry nitrogen, confirming that the change in thickness is due to absorption of moisture (Figure?). Increasing the pressure too high reduces the image quality and therefore we could only increase the pressure until 44.8% RH. We found that the thickness scales linearly with pressure and, assuming a linear relationship between thickness and RH, we predict that the thickness of the SMNP film should increase by 17.4 % when increasing the RH from 10% to 90%.

A standard thin film interference model[16] was used to calculate the reflectance spectra for both blue and red SMNP films. We measured the refractive index and extinction coefficient of SMNP in our previous work and we assume the volume fraction of SMNP film is 55%.[14] At RH of 10%, the thickness of SMNP films should be greater than that measured using SEM and we increased the thickness of SMNP from the value from SEM measurement until the maximum peak position matches well with experimental reflectance curves (Figure 5a and 5b). The thickness for blue and red film is 327 nm and 652 nm at RH of 10%, respectively. With increase of the RH to 90%, adsorption of water vapor will not only swell the film but also decrease the effective refractive index of SMNPs. Based on the thickness expansion ratio of 17.4% from RH of 10% to 90% measured by ESEM, the thickness for blue and red film at RH of 90% is calculated to be 384 nm and 765 nm, respectively. We fit the new refractive index of SMNP at RH of 90% to match the model spectra with experimental curves (Figure 5c and 5d) and we obtain RI for wet SMNP is 1.64, which is smaller than 1.74 at RH of 10%.
We also quantified how much water was adsorbed by measuring the changes in mass as a function of humidity. Figure 6 shows water uptake weight percentage increases linearly with increase in RH. Assuming a linear fit, we predict the water uptake mass weight (ω) to be 13% when increasing the RH from 10% to 90%. The increase of SMNP in volume relative to SMNPs can be calculated using the following expression:

$$V_{water} = \rho_{smnp} V_{smnp} \omega = 0.169 V_{smnp}$$

Where ρ_{smnp} and V_{smnp} are the density and volume of the SMNP in the film, respectively. A SMNP film can adsorb water of 16.9% in volume with increasing RH from 10% to 90%, and its thickness swells by 17.4% from ESEM measurements. Therefore, water adsorption by SMNP will cause nanoparticles to swell only in one dimension, which suggest anisotropic swelling of nanoparticles.
Here, SMNPs make it possible to achieve rapid and substantial color response with humidity without using any additional hygroscopic materials for water adsorption or inorganic component to increase refractive index contrast. We can define the sensitivity of the color change to the humidity as follows:

$$S = \frac{\text{peak shift (nm)}}{\text{water uptake (\%)}}$$

For our SMNP films, only 13 % water adsorption in mass can lead to 77 nm color shifts, therefore S is 5.9 nm / 1%, which is much larger than that those reported for polymer electrolyte films (2.2 nm /1%, 195 nm shift in max peak is achieved with 90% water uptake). _ENREF_14[17] With lower water uptake, the SMNP is more likely to avoid structural deterioration after multiple wetting and drying cycles. Relative to 1D multilayer structures, SMNP film doesn't require several types of coating procedures and more importantly, the SMNP film has some porosity between closed packed particles, making it adsorb/desorb water vapor more rapidly than solid films.

Conclusions

We have produced bio-inspired SMNP films that change color in response to humidity. We controlled the thickness of SMNP films to obtain colors from blue to green at RH of 10%. Both blue and red films quickly turned to green with maximum peak position shift in the reflectance spectrum up to 76 nm when increasing RH from 10% to 90%. Such humidity-induced color changes are reversible and durable after many cycles. We combined experimental evidence from ESEM and theoretical thin-film optical model to demonstrate that the high humidity (90%) swells SMNP film along thickness direction by 17% and reduces refractive index of SMNP to 1.64 from 1.74, leading to the color changes. The one

dimensional swelling behavior is also confirmed by simple water uptake measurements. Use of SMNPs is critical to production of these dynamic colors because of its high refractive index that enables greater sensitivity of color change. Films made of moderate hydroscopic SMNP have porosity to obtain rapid and cyclic humidity response. In the future, an in-depth study of the water interaction with SMNP at molecular level is necessary for developing novel optical devices out of SMNP-based materials.

Reference

1. Hsiung, B.-K.; Deheyn, D. D.; Shawkey, M. D.; Blackledge, T. A. Blue reflectance in tarantulas is evolutionarily conserved despite nanostructural diversity. *Science Advances* 2015, 1, e1500709.
2. Umbers, K. D.; Fabricant, S. A.; Gawryszewski, F. M.; Seago, A. E.; Herberstein, M. E. Reversible colour change in Arthropoda. *Biological Reviews* 2014, 89, 820-848.
3. Mäthger, L. M.; Denton, E. J.; Marshall, N. J.; Hanlon, R. T. Mechanisms and behavioural functions of structural coloration in cephalopods. *J. R. Soc. Interface* 2009, 6, S149-S163.
4. Potyrailo, R. A.; Ghiradella, H.; Vertiatchikh, A.; Dovidenko, K.; Cournoyer, J. R.; Olson, E. Morpho butterfly wing scales demonstrate highly selective vapour response. *Nat. Photonics* 2007, 1, 123-128.
5. Eliason, C. M.; Shawkey, M. D. Rapid, reversible response of iridescent feather color to ambient humidity. *Opt. Express* 2010, 18, 21284-21292.
6. Rassart, M.; Colomer, J.; Tabarrant, T.; Vigneron, J. Diffractive hygrochromic effect in the cuticle of the hercules beetle Dynastes hercules. *New Journal of Physics* 2008, 10, 033014.
7. Wang, Z.; Zhang, J.; Xie, J.; Li, C.; Li, Y.; Liang, S.; Tian, Z.; Wang, T.; Zhang, H.; Li, H. Bioinspired Water-Vapor-Responsive Organic/Inorganic Hybrid One-Dimensional Photonic Crystals with Tunable Full-Color Stop Band. *Adv. Funct. Mater.* 2010, 20, 3784-3790.
8. Karaman, M.; Kooi, S. E.; Gleason, K. K. Vapor deposition of hybrid organic–inorganic dielectric Bragg mirrors having rapid and reversibly tunable optical reflectance. *Chem. Mater.* 2008, 20, 2262-2267.
9. Szendrei, K.; Ganter, P.; Sànchez-Sobrado, O.; Eger, R.; Kuhn, A.; Lotsch, B. V. Touchless Optical Finger Motion Tracking Based on 2D Nanosheets with Giant Moisture Responsiveness. *Adv. Mater.* 2015, 27, 6341-6348.
10. Tian, E.; Wang, J.; Zheng, Y.; Song, Y.; Jiang, L.; Zhu, D. Colorful humidity sensitive photonic crystal hydrogel. *J. Mater. Chem.* 2008, 18, 1116-1122.
11. Barry, R. A.; Wiltzius, P. Humidity-sensing inverse opal hydrogels. *Langmuir* 2006, 22, 1369-1374.
12. Xuan, R.; Wu, Q.; Yin, Y.; Ge, J. Magnetically assembled photonic crystal film for humidity sensing. *J. Mater. Chem.* 2011, 21, 3672-3676.
13. Diao, Y. Y.; Liu, X. Y.; Toh, G. W.; Shi, L.; Zi, J. Multiple Structural Coloring of Silk-Fibroin Photonic Crystals and Humidity-Responsive Color Sensing. *Adv. Funct. Mater.* 2013, 23, 5373-5380.
14. Xiao, M.; Li, Y.; Allen, M. C.; Deheyn, D. D.; Yue, X.; Zhao, J.; Gianneschi, N. C.; Shawkey, M. D.; Dhinojwala, A. Bio-Inspired Structural Colors Produced via Self-Assembly of Synthetic Melanin Nanoparticles. *ACS Nano* 2015, 9, 5454-5460.
15. Starr, C. *Biology: concepts and applications*. 7th ed.; Cengage Learning: Stamford, CT, 2007.
16. Azzam, R. M.; Bashara, N. M. *Ellipsometry And Polarized Light*. North-Holland: Amsterdam, Netherland, 1977.
17. Kim, E.; Kim, S. Y.; Jo, G.; Kim, S.; Park, M. J. Colorimetric and resistive polymer electrolyte thin films for real-time humidity sensors. *ACS Appl. Mater. Interfaces* 2012, 4, 5179-5187.

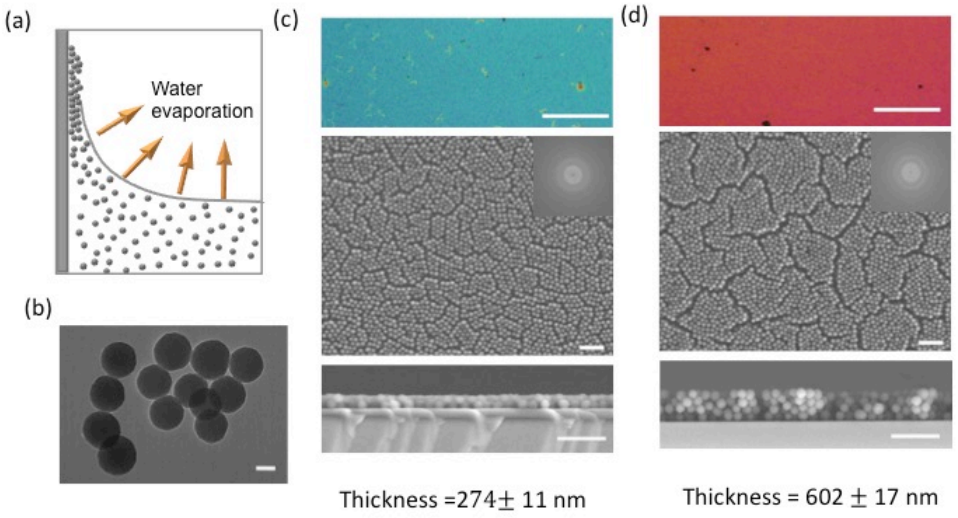

Figure 1. (a) Scheme of evaporation induced self-assembly process. (b) TEM image of SMNPs, scale bar 100 nm. Optical Images, Top view and side view SEM images for blue (c) and red (d) SMNP films. Scale bars, 100 μm for optical images and 1 μm for SEM images.

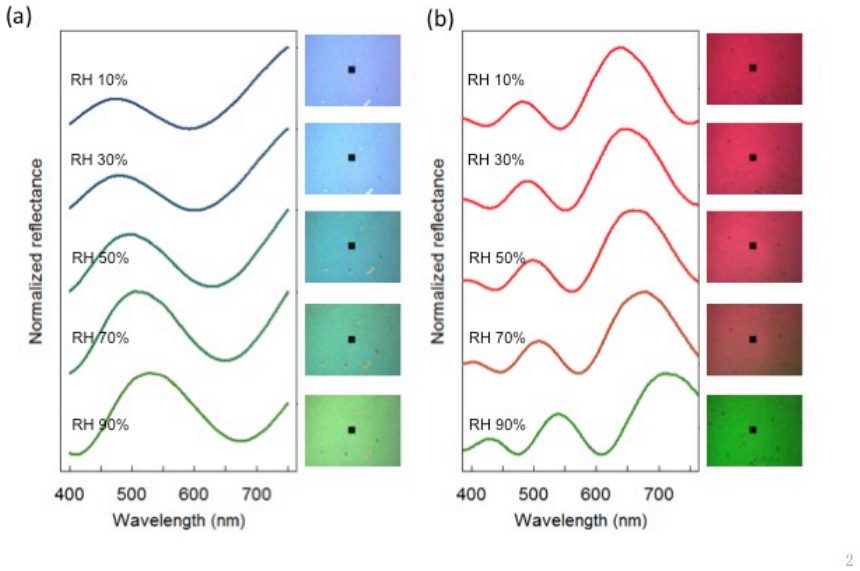

Figure 2. Changes of reflectance spectra and colors for blue (a) and red (b) films at RH of 10%, 30%, 50%, 70% and 90%.

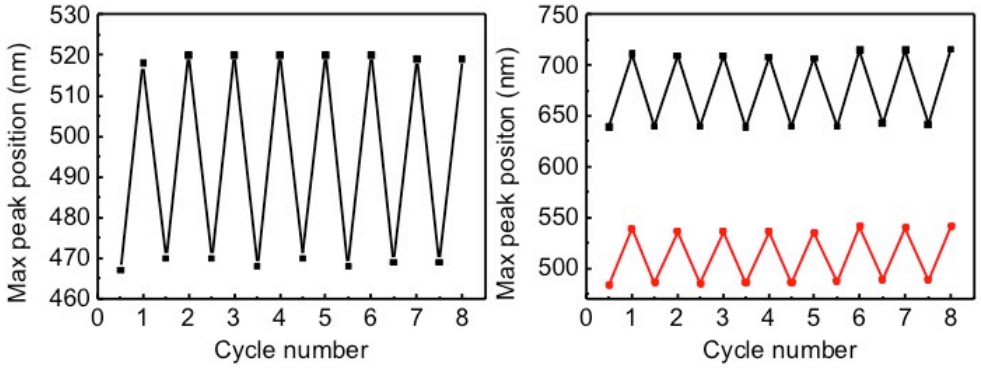

Figure 3. Maximum peak positions in the spectra of blue film (a) and red film (b) within visible range change during 8 times of drying and wetting cycles.

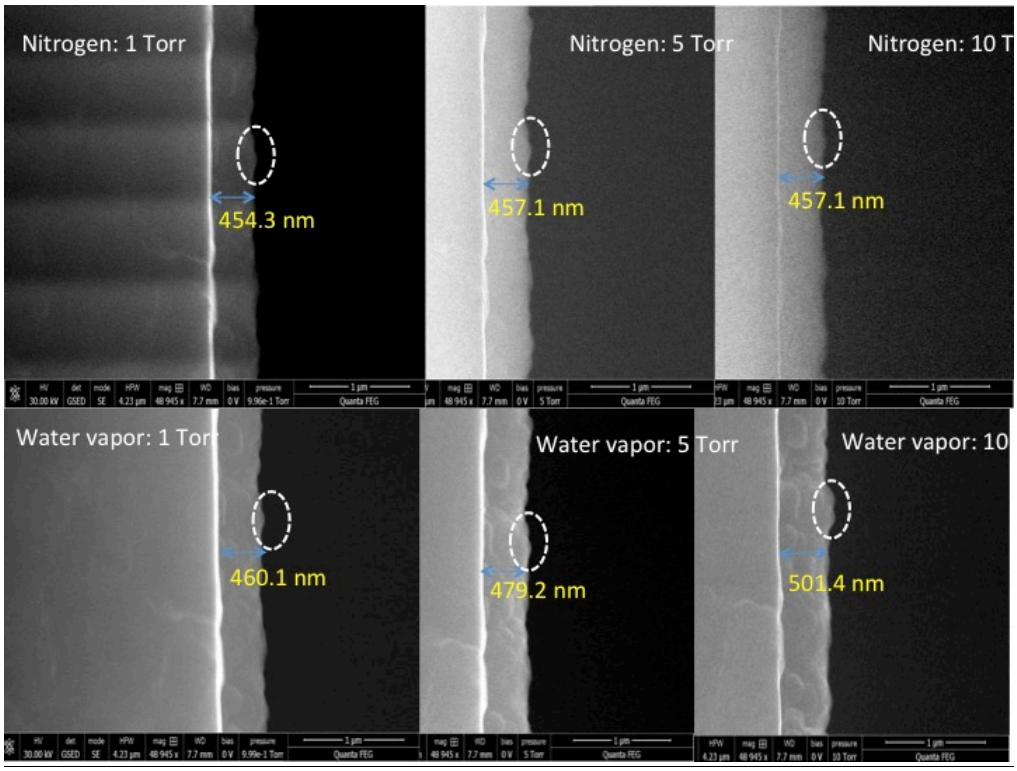

Figure 4. Environmental SEM on cross section of a SMNP film under dry N_2 (a) and water vapor (b) conditions at various pressures (1 Torr, 5 Torr and 10 Torr).

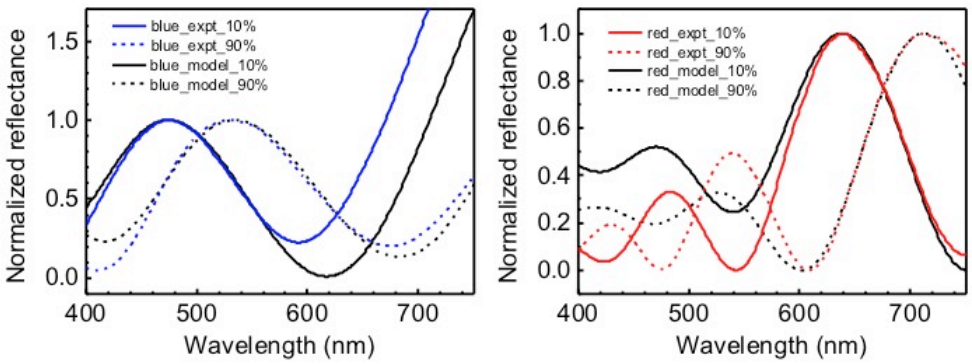

Figure 5. (a) Measured spectra (blue color) and model spectra (black color) for blue film at RH of 10% (solid) and 90% (dotted). (b) Measured spectra (red color) and model spectra (black color) for red film at RH of 10% (solid) and 90% (dotted).

Publications (23 total)

B. Hsiung, D. Deheyn, **M.D. SHAWKEY,** and T.A. Blackledge. 2015. Blue color in tarantulas is evolutionarily conserved despite nanostructural diversity. *Science Advances* 1: e1500709

(Received press coverage in *National Geographic, The Atlantic, The Verge, BBC News*, *Science News*, *Science, The Independent* and numerous other outlets)

B. Hsiung, T.A. Blackledge, and **M.D. SHAWKEY.** 2015. Spiders do have melanin after all. *Journal of Experimental Biology* 218:3632-3635.

B. Igic, E. Zarate, M. A. Sewell, C. Moskát, P. Cassey, J. Rutila, T. Grim, **M.D. SHAWKEY**, and M. E. Hauber. 2015. A comparison of egg yolk lipid components between parasitic Common Cuckoos and their hosts. *The Auk: Ornithological Advances* 132:817-825.

(cover article)

M.E. Hauber, Z. Aidala, B.Igic, **M.D. SHAWKEY**, and C. Moskát. 2015. Orange is not the new green: Experimental shifts in nest-egg contrasts do not predict egg rejection decisions by great reed warbler hosts of brood parasitic common cuckoos. *Animal Cognition* DOI 10.1007/s10071-015-0886-9.

M. Xiao, Y. Li, M. Allen, D. Deheyn, X. Yue, J, Zhao, N. Gianneschi, **M.D. SHAWKEY,** and A. Dhinojwala. 2015. Bio-inspired structural colors produced via self-assembly of synthetic melanin nanoparticles. *ACS Nano* 9:5454-5460.

(Named as Editor's Choice in *ACS Nano*. Received press coverage in *Popular Science, Chemical and Engineering News*, *Red Orbit* and other outlets.)

B. Igic, V.Nunez, H.U. Voss, R. Croston, Z. Aidala, A. Lopez, A.Van Tatenhove, M. Holford, **M.D. SHAWKEY**, and M.E. Hauber. 2015. Examining egg-rejection behavior of wild birds using 3D printed eggs. *PeerJ* 3:e965 https://dx.doi.org/10.7717/peerj.965.

(Received extensive press coverage in numerous outlets, including *Washington Post, Popular Science, Forbes, Science, Audubon Magazine*)

D. C. Fecheyr-Lippens, B. Igic, L. D'Alba, D. Hanley, A. Verdes, M. Holford, G.I.N. Waterhouse, T. Grim, M.E. Hauber, and **M.D. SHAWKEY.** 2015. The cuticle modulates ultraviolet reflectance of avian eggshells. *Biology Open* doi:10.1242/bio.01221.

L. D'Alba and **M.D. SHAWKEY**. 2015. Antimicrobial defenses in avian eggs: a review. *J. Ornithology.* DOI:0.1007/s10336-015-1226-1

C.M. Eliason, ***R. Maia***, and **M.D. SHAWKEY.** 2015. Modular color evolution in birds facilitated by a complex nanostructure. *Evolution* 69: 357-367.

(Received press coverage in *Chemical and Engineering News*)

M.E. Hauber, L.Tong, M. Bán, R. Croston, T. Grim, G.I.N. Waterhouse, **M.D. SHAWKEY**, and C. Moskát. 2015. The value of artificial stimuli in behavioral ecology research: Making the case for egg rejection studies in avian brood parasitism. *Ethology* DOI: 10.1111/eth.12359.

B. Igic, ***Daphne Fecheyr-Lippens***, A. Chan, D. Hanley, P. Brennan, T. Grim, G.I.N. Waterhouse, M.E. Hauber, and **M.D. SHAWKEY.** 2015. A nanostructural basis for gloss of avian eggshells. *Journal of the Royal Society Interface* DOI: 10.1098/rsif.2014.1210

(Received press coverage in numerous outlets, including *New York Times, National Geographic, Discover, VICE, Physics World*)

M.D. SHAWKEY, L. D'Alba, ***M. Xiao***, M. Schutte and R. Buchholz. 2015. Ontogeny of an iridescent nanostructure composed of hollow melanosomes. *Journal of Morphology*. doi: 10.1002/jmor.20347

B. Hsiung, T.A. Blackledge and **M.D. SHAWKEY.** 2014. Structural color and its interactions with other color-producing elements: perspectives from spiders. *Proceedings of SPIE.*9187, The Nature of Light: Light in Nature V, 91870B (8 September 2014); doi: 10.1117/12.2060831

S. Liu, **M.D. SHAWKEY,** D. Parkinson and M. Ahmed. 2014. Elucidation of the chemical composition of avian melanin. *Royal Society of Chemistry Advances* 4: 40396-40399.

L. D'Alba, C. van Hemert, K.A. Spencer, B.J. Heidinger, L. Gill, N.P. Evans, P. Monaghan, C.M. Handel, and **M.D. SHAWKEY.** 2014. Melanin-based color of plumage: Role of condition and of feathers' microstructure. *Integrative and Comparative Biology* doi: 10.1093/icb/icu094

M. Xiao, Ali Dhinojwala and **M.D. SHAWKEY.** 2014. Nanostructural basis of rainbow-like iridescence in common bronzewing *Phaps chalcoptera* feathers. *Optics Express* 22:14625-14636.

C. M. Eliason and **M.D. SHAWKEY.** 2014. Antireflection-enhanced color by a natural graded refractive index (GRIN) structure. *Optics Express* 22:A642-A650.

J. Prokop, C. Schmidt, D. Gasper, R.J. Duff, A. Milsted, T. Ohkubo, H.C. Ball, **M.D. SHAWKEY**, H.L. Mays, L.A. Cogburn, R.L. Londraville. 2014. Discovery of the elusive leptin in birds: identification of several "missing links" in the evolution of leptin and its receptor. *PLoS ONE* 9:e92751

L. D'Alba, ***C.M. Eliason***, H. Badawy, D.N. Jones and **M.D. SHAWKEY.** 2014. Antimicrobial effects of a nanostructured eggshell in a compost-nesting bird. *Journal of Experimental Biology* 217:1116-1121.

(cover article, press coverage in *Nature*)

Q. Li, J.A. Clarke*, K. Gao, C. Zhou, Q. Meng, D. Li, L. D'Alba and **M.D. SHAWKEY*.** 2014. Melanosome evolution indicates a key physiological shift within feathered dinosaurs. *Nature.* Doi:10.1038/nature12973
***Co-corresponding authors**

(Received press coverage in *National Geographic, Time, Smithsonian Magazine, ABC News, Discovery Channel News* and numerous other outlets)

J. Lindgren, P. Sjovall, J.A. Gren, P. Udval, G. Dyke, R.M. Carney, B.P. Schultz, **M.D. SHAWKEY**, K.R. Barnes, and M.J. Polcyn. 2014. Skin pigmentation provides evidence of convergent melanism in extinct marine reptiles. *Nature.* doi:10.1038/nature12899

*(*Article featured in front cover text. Received extensive press coverage in *National Geographic, BBC News, Popular Mechanics, Discover Magazine* and numerous other outlets*)*

C. M. Eliason, P.P. Bitton and **M.D. SHAWKEY.** 2013. How hollow melanosomes affect iridescent colour production in birds. *Proceedings of the Royal Society of London B.* DOI:10.1098/rspb.2013.1505

***R. Maia*,** D.R. Rubenstein and **M.D. SHAWKEY.** 2013. Key ornamental innovations facilitate diversification in an avian radiation. *Proceedings of the National Academy of Sciences USA* DOI: 10.1073/pnas.1220784110

Interactions

Nathan Gianneschi (UCSD)- Collaboration on self-assembly of synthetic melanosomes. Co-authored one publication

Dimitri Deheyn (Scripps)- Collaborations on synthetic melanosomes, spider color. Co-authored two publications

Alamgir Karim (University of Akron)Self-assembly of optical nanostructures through phase separation. Co-advise PhD student Asritha Nallapaneni

Ali Dhinojwala (U. Akron) Polymer science of nanostructures, synthesis of iridescent feather mimics. Co-advise PhD student Ming Xiao

Todd Blackledge (U. Akron) Collaboration on spider color. Co-advise PhD student Bill Hsiung.

Musa Ahmed (Lawrence Berkeley National Lab) Collaboration on melanin chemistry

Transitions

-Use of synthetic melanin nanoparticles produced by Nathan Gianneschi's group to produce structural colors
- Collaboration with Musa Ahmed on chemical characterization of natural melanin.

Evolutionary Aspects
-Characterization of optics/structure of biophotonic nanostructures.
-Identify new biophotonic nanostructures/optical mechanisms

Transformative Aspects
-Tracing the development of biophotonic nanostructures in living organisms.
-Identify the role of hierarchical self-assembly could create new empirically supported paradigm of development of highly ordered biophotonic nanostructures.
-Production of new self-assembled photonic nanostructures using natural materials with unique optical properties.

AFOSR Deliverables Submission Survey

Response ID:5709 Data

1.

1. Report Type

Final Report

Primary Contact E-mail
Contact email if there is a problem with the report.

shawkey@uakron.edu

Primary Contact Phone Number
Contact phone number if there is a problem with the report

+32-9-264-53-24

Organization / Institution name

University of Akron

Grant/Contract Title
The full title of the funded effort.

CHARACTERIZATION AND BIOMIMCRY OF AVIAN NANOSTRUCTURED TISSUES

Grant/Contract Number
AFOSR assigned control number. It must begin with "FA9550" or "F49620" or "FA2386".

FA9550-13-1-0222

Principal Investigator Name
The full name of the principal investigator on the grant or contract.

Matthew D Shawkey

Program Manager
The AFOSR Program Manager currently assigned to the award

Hugh DeLong

Reporting Period Start Date

09/30/2013

Reporting Period End Date

12/18/2015

Abstract

Research resulting from these projects has resulted in 23 peer-reviewed papers, many featuring post-docs and graduate students funded by this grant. We have received significant press attention for some of these papers, including coverage in the New York TImes, Washington Post, National Geographic, and Chemical and Engineering News. Two graduate students funded by the grant graduated and are now post-docs. An open-source software package for analyzing spectral data (PAVO), developed in part using these funds, was released and has been extensively used throughout the world. PI Shawkey was selected as a Kavli Fellow of the National Academy of Sciences.

Understanding the properties and development of complex morphological traits may spark advances in the biomimetic design of new self-assembling multifunctional materials. Thus, we are using cutting-edge techniques to (I) identify previously

unexplored chemical and physical properties of, and (II) synthetically mimic, color-producing nanostructures built from keratin and melanin in bird feathers.

For (I) we are testing four properties of optical nanostructures: (1) Refractive index and chemistry. We use plasmonics to measure refractive index of melanins and synchrotron-based Vacuum Ultraviolet Laser Desorption Mass Spectrometry techniques to compare their chemistry. We have optimized techniques for measurement of refractive index and have made significant progress understanding the chemistry that contributes to variation in color of feathers. (2) Tensile strength. We use atomic force microscopy to quantify how both the morphology and chemistry of individual melanosomes, as well as their organization into nanostructures, affects their material properties. We have a full dataset on tensile strength of iridescent barbules, and are currently collecting one on non-iridescent barbules for comparison (3) Thermoregulation. We use Fourier transform Infrared Spectroscopy and infrared imaging techniques to test how the wavelength selectivity caused by the organization of melanosomes into nanostructures affects absorbance. (4) Hydrophobicity. We use contact angle goniometry and modeling to determine how macrostructural modifications associated with nanostructures may affect hydrophobicity and directional water movement on feathers. We have identified nanostructured surfaces that create bright white color and superhydrophobicity.
For part (II) we use biomimetic approaches to elucidate the mechanisms by which these nanostructures self assemble. First, we replicate the depletion attraction forces that cause melanosomes to self assemble into iridescent nanostructures through a series of experiments in which we vary the conditions of polymerization of keratin and melanin blends. We have succeeded in organizing melanin particles into simple nanostructures, and are proceeding with experiments using blends and modified particle types. Second, we replicate the phase separation processes that cause self-assembly of non-iridescent nanostructures by producing keratin films from both nanostructured and unstructured keratin under varying conditions, and will identify differences in primary sequence or phosphorylation state between nanostructured and unstructured keratin. The results of this research will enhance our understanding of the multifunctionality of nanostructured traits and identify new means and natural materials for their production.

Distribution Statement
This is block 12 on the SF298 form.

Distribution A - Approved for Public Release

Explanation for Distribution Statement
If this is not approved for public release, please provide a short explanation. E.g., contains proprietary information.

SF298 Form
Please attach your SF298 form. A blank SF298 can be found here. Please do not password protect or secure the PDF The maximum file size for an SF298 is 50MB.

SF298_Shawkey.pdf

Upload the Report Document. File must be a PDF. Please do not password protect or secure the PDF . The maximum file size for the Report Document is 50MB.

shawkey_afosr_final_2016_small.pdf

Upload a Report Document, if any. The maximum file size for the Report Document is 50MB.

Archival Publications (published) during reporting period:

C.M. Eliason, M.D. SHAWKEY, and J.A. Clarke. In press. Evolutionary shifts in the melanin-based color systems of birds. Evolution

M.D. SHAWKEY and L. D'Alba. In press. Paleocolor: the mechanisms and evolution of plumage color in birds and other dinosaurs. For Mesozoic Birds II (L. Chiappe, Ed.)

B. Hsiung, D. Deheyn, M.D. SHAWKEY, and T.A. Blackledge. 2015. Blue color in tarantulas is evolutionarily conserved despite nanostructural diversity. Science Advances 1: e1500709

(Received press coverage in National Geographic, The Atlantic, The Verge, BBC News, Science News, Science, The Independent and numerous other outlets)

B. Hsiung, T.A. Blackledge, and M.D. SHAWKEY. 2015. Spiders do have melanin after all. Journal of Experimental Biology 218:3632-3635.

B. Igic, E. Zarate, M. A. Sewell, C. Moskát, P. Cassey, J. Rutila, T. Grim, M.D. SHAWKEY, and M. E. Hauber. 2015. A comparison of egg yolk lipid components between parasitic
Common Cuckoos and their hosts. The Auk: Ornithological Advances 132:817-825.

(cover article)

M.E. Hauber, Z. Aidala, B.Igic, M.D. SHAWKEY, and C. Moskát. 2015. Orange is not thenew green: Experimental shifts in nest-egg contrasts do not predict egg rejection decisions by great reed warbler hosts of brood parasitic common cuckoos. Animal Cognition DOI 10.1007/s10071-015-0886-9.

M. Xiao, Y. Li, M. Allen, D. Deheyn, X. Yue, J, Zhao, N. Gianneschi, M.D. SHAWKEY, and A. Dhinojwala. 2015. Bio-inspired structural colors produced via self-assembly of synthetic melanin nanoparticles. ACS Nano 9:5454-5460.

(Named as Editor's Choice in ACS Nano. Received press coverage in Popular Science, Chemical and Engineering News, Red Orbit and other outlets.)

B. Igic, V.Nunez, H.U. Voss, R. Croston, Z. Aidala, A. Lopez, A.Van Tatenhove, M. Holford, M.D.SHAWKEY, and M.E. Hauber. 2015. Examining egg-rejection behavior of wild birds using 3D printed eggs. PeerJ 3:e965 https://dx.doi.org/10.7717/peerj.965.

(Received extensive press coverage in numerous outlets, including Washington Post, Popular Science, Forbes, Science, Audubon Magazine)

D. C. Fecheyr-Lippens, B. Igic, L. D'Alba, D. Hanley, A. Verdes, M. Holford, G.I.N. Waterhouse, T. Grim, M.E. Hauber, and M.D. SHAWKEY. 2015. The cuticle modulates ultraviolet reflectance of avian eggshells. Biology Open doi:10.1242/bio.01221.

L. D'Alba and M.D. SHAWKEY. 2015. Antimicrobial defenses in avian eggs: a review. J. Ornithology. DOI:0.1007/s10336-015-1226-1

C.M. Eliason, R. Maia, and M.D. SHAWKEY. 2015. Modular color evolution in birds facilitated by a complex nanostructure. Evolution 69: 357-367.

(Received press coverage in Chemical and Engineering News)

M.E. Hauber, L.Tong, M. Bán, R. Croston, T. Grim, G.I.N. Waterhouse, M.D. SHAWKEY, and C. Moskát. 2015. The value of artificial stimuli in behavioral ecology research: Making the case for egg rejection studies in avian brood parasitism. Ethology DOI: 10.1111/eth.12359.

B. Igic, Daphne Fecheyr-Lippens, A. Chan, D. Hanley, P. Brennan, T. Grim, G.I.N. Waterhouse, M.E. Hauber, and M.D. SHAWKEY. 2015. A nanostructural basis for gloss of avian eggshells. Journal of the Royal Society Interface DOI: 10.1098/rsif.2014.1210

(Received press coverage in numerous outlets, including New York Times, National
Geographic, Discover, VICE, Physics World)

M.D. SHAWKEY, L. D'Alba, M. Xiao, M. Schutte and R. Buchholz. 2015. Ontogeny of an iridescent nanostructure composed of

hollow melanosomes. Journal of Morphology. doi: 10.1002/jmor.20347

B. Hsiung, T.A. Blackledge and M.D. SHAWKEY. 2014. Structural color and its interactions with other color-producing elements: perspectives from spiders. Proceedings of SPIE.9187, The Nature of Light: Light in Nature V, 91870B (8 September 2014); doi: 10.1117/12.2060831

S. Liu, M.D. SHAWKEY, D. Parkinson and M. Ahmed. 2014. Elucidation of the chemical composition of avian melanin. Royal Society of Chemistry Advances 4: 40396-40399.

L. D'Alba, C. van Hemert, K.A. Spencer, B.J. Heidinger, L. Gill, N.P. Evans, P. Monaghan, C.M. Handel, and M.D. SHAWKEY. 2014. Melanin-based color of plumage: Role of condition and of feathers' microstructure. Integrative and Comparative Biology doi: 10.1093/icb/icu094

M. Xiao, Ali Dhinojwala and M.D. SHAWKEY. 2014. Nanostructural basis of rainbow-like iridescence in common bronzewing Phaps chalcoptera feathers. Optics Express 22:14625-
14636.

C. M. Eliason and M.D. SHAWKEY. 2014. Antireflection-enhanced color
by a natural graded refractive index (GRIN) structure. Optics Express 22:A642-A650.

J. Prokop, C. Schmidt, D. Gasper, R.J. Duff, A. Milsted, T. Ohkubo, H.C. Ball, M.D. SHAWKEY, H.L. Mays, L.A. Cogburn, R.L. Londraville. 2014. Discovery of the elusive leptin in birds: identification of several "missing links" in the evolution of leptin and its receptor. PLoS ONE 9:e92751

L. D'Alba, C.M. Eliason, H. Badawy, D.N. Jones and M.D. SHAWKEY. 2014. Antimicrobial effects of a nanostructured eggshell in a compost-nesting bird. Journal of Experimental Biology 217:1116-1121.

(cover article, press coverage in Nature)

Q. Li, J.A. Clarke*, K. Gao, C. Zhou, Q. Meng, D. Li, L. D'Alba and M.D. SHAWKEY*. 2014. Melanosome evolution indicates a key physiological shift within feathered dinosaurs.
Nature. Doi:10.1038/nature12973
*Co-corresponding authors

(Received press coverage in National Geographic, Time, Smithsonian Magazine, ABC News, Discovery Channel News and numerous other outlets)

J. Lindgren, P. Sjovall, J.A. Gren, P. Udval, G. Dyke, R.M. Carney, B.P. Schultz, M.D. SHAWKEY, K.R. Barnes, and M.J. Polcyn. 2014. Skin pigmentation provides evidence of convergent melanism in extinct marine reptiles. Nature.
doi:10.1038/nature12899

(Article featured in front cover text. Received extensive press coverage in National Geographic, BBC News, Popular Mechanics, Discover Magazine and numerous other outlets)

Changes in research objectives (if any):

None

Change in AFOSR Program Manager, if any:

None

Extensions granted or milestones slipped, if any:

AFOSR LRIR Number

LRIR Title

Reporting Period

Laboratory Task Manager

Program Officer

Research Objectives

Technical Summary

Funding Summary by Cost Category (by FY, $K)

	Starting FY	FY+1	FY+2
Salary			
Equipment/Facilities			
Supplies			
Total			

Report Document

Report Document - Text Analysis

Report Document - Text Analysis

Appendix Documents

2. Thank You

E-mail user

Jan 19, 2016 04:33:23 Success: Email Sent to: shawkey@uakron.edu

Response ID: 5709

Survey Submitted:	Jan 19, 2016 4:33 AM
IP Address:	157.193.240.224
Language:	English (en-US,en;q=0.8)
User Agent:	Mozilla/5.0 (Macintosh; Intel Mac OS X 10_6_8) AppleWebKit/537.36 (KHTML, like Gecko) Chrome/47.0.2526.111 Safari/537.36
Http Referrer:	http://afosr.reports.sgizmo.com/s3
Page Path:	1 : (SKU: 1) 2 : Thank You (SKU: 2)

SessionID:	1453193431_569df8d7d2fd55.16845550

Response Location

Country:	Belgium
Region:	08
City:	Gent
Postal Code:	9000
Long & Lat:	Lat: 51.049999237061, Long:3.7167000770569